

 Open access • Posted Content • DOI:10.1101/2020.06.02.128702

## Neuronal activity in sensory cortex predicts the specificity of learning.

— [Source link](#) 

Katherine C. Wood, Christopher F. Angeloni, Karmi Oxman, Claudia Clopath ...+1 more authors

**Institutions:** University of Pennsylvania, Imperial College London

**Published on:** 03 Jun 2020 - bioRxiv (Cold Spring Harbor Laboratory)

**Topics:** Fear conditioning, Associative learning, Stimulus (physiology), Sensory system and Population

Related papers:

- [Neural signature of delayed fear generalization under stress](#)
- [Differential fear conditioning generates prefrontal neural ensembles of safety signals.](#)
- [Graded fear generalization enhances the level of cfos-positive neurons specifically in the basolateral amygdala.](#)
- [Noradrenergic stimulation increases fear memory expression.](#)
- [An organization of visual and auditory fear conditioning in the lateral amygdala](#)

Share this paper:    

View more about this paper here: <https://typeset.io/papers/neuronal-activity-in-sensory-cortex-predicts-the-specificity-27p3j89h1n>

1 **Title: Neuronal activity in sensory cortex predicts the specificity of**  
2 **learning.**

3

4

5 Authors: Katherine C. Wood<sup>1</sup>, Christopher F. Angeloni<sup>1,2</sup>, Karmi Oxman<sup>1</sup>, Claudia Clopath<sup>4</sup>,  
6 \*Maria N. Geffen<sup>1,2,3</sup>

7

8 Affiliations: <sup>1</sup>Departments of Otorhinolaryngology: Head and Neck Surgery, University of  
9 Pennsylvania

10 <sup>2</sup>Department of Psychology, University of Pennsylvania

11 <sup>3</sup>Departments of Neurology and Neuroscience, University of Pennsylvania

12 <sup>4</sup>Department of Bioengineering, Imperial College London

13

14 \*Lead and corresponding Author:

15 Maria N. Geffen: [mgeffen@pennmedicine.upenn.edu](mailto:mgeffen@pennmedicine.upenn.edu)

16

17

## 18 **Abstract**

19            Learning to avoid dangerous signals while preserving normal responses to safe stimuli is  
20 essential for everyday behavior and survival. Fear learning has a high level of inter-subject  
21 variability. Following identical experiences, subjects exhibit fear specificities ranging from high  
22 (specializing fear to only the dangerous stimulus) to low (generalizing fear to safe stimuli).  
23 Pathological fear generalization underlies emotional disorders, such as post-traumatic stress  
24 disorder. The neuronal basis of fear specificity remains unknown. Here, we identified the  
25 neuronal code that underlies inter-subject variability in fear specificity using longitudinal imaging  
26 of neuronal activity before and after differential fear conditioning in the auditory cortex of mice.  
27 Neuronal activity prior to, but not after learning predicted the level of specificity following fear  
28 conditioning across subjects. Stimulus representation in auditory cortex was reorganized  
29 following conditioning. However, the reorganized neuronal activity did not relate to the specificity  
30 of learning. These results present a novel neuronal code that determines individual patterns in  
31 learning.

32            Keywords: fear conditioning, auditory cortex, sensory systems, learning, computational  
33 model, imaging, sensory cortex, tuning curve, neurobiology, population coding.

34

## 35 Introduction

36 Learning allows our brain to adjust sensory representations based on environmental  
37 demands. Fear conditioning, in which a neutral stimulus is paired with an aversive stimulus, is a  
38 robust form of associative learning: exposure to just a few stimuli can lead to a fear response  
39 that lasts over the subject's lifetime<sup>1,2</sup>. However, the same fear conditioning paradigm elicits  
40 different levels of learning specificity across subjects<sup>3-6</sup>. In pathological cases, the  
41 generalization of the fear response to stimuli in non-threatening situations can lead to conditions  
42 such as post-traumatic stress disorder (PTSD)<sup>7,8</sup> and anxiety<sup>9</sup>. Therefore, determining the  
43 neuronal basis for learning specificity following fear conditioning is important and can lead to  
44 improved understanding of the neuropathology of these disorders. Whereas much is known  
45 about how fear is associated with the paired stimulus, the neuronal mechanisms that determine  
46 the level of specificity of fear learning remain poorly understood. Our first goal was to determine  
47 the neuronal basis for the differential fear learning specificity across subjects.

48 Multiple studies suggest the auditory cortex (AC) is involved in fear learning. *During*  
49 differential fear conditioning (DFC), inactivation of AC chemically<sup>10</sup>, or with optogenetics<sup>11</sup>, as  
50 well as partial suppression of inhibition in AC<sup>12</sup> led to decreased learning specificity using either  
51 pure tones or complex stimuli, such as FM sweeps or vocalizations<sup>3,11-14</sup>. These observations  
52 suggest that AC may determine the level of learning specificity. Therefore, we tested whether  
53 neuronal codes in AC *prior* to conditioning can predict specificity of fear learning.

54 The role of AC *following* fear conditioning is more controversial. Changes in stimulus  
55 representation in AC following association learning have been proposed to represent multiple  
56 different features of the fear response<sup>1,14-19</sup>. However, inactivation of the auditory cortex did not  
57 affect fear memory retrieval of pure tones<sup>3,11</sup>, suggesting that AC is not involved in fear memory  
58 retrieval. If AC were involved in fear memory retrieval, we would expect the changes in sound  
59 representation to reflect the level of learning specificity across subjects. Therefore, our second  
60 goal was to test the role of changes in auditory cortex in shaping fear learning specificity across  
61 subjects.

62 To address these goals, we imaged the activity of neuronal ensembles in layers 2 and 3 of  
63 AC over weeks, before and after differential fear conditioning with pure tones. First, we  
64 established the neuronal basis for differential learning specificity across subjects by finding that  
65 neuronal activity in AC prior to fear conditioning predicted the level of learning specificity.

66 Second, we found that the changes in stimulus representation in AC following fear conditioning  
67 were not correlated with the level of learning specificity across subjects, suggesting that the role  
68 of AC in fear learning is restricted to the consolidation period and changes in AC do not represent  
69 fear memory. These findings refine our understanding of the neuronal code for variability in fear  
70 learning across subjects and reconcile seemingly conflicting previous results on the function of  
71 the auditory cortex in fear learning.

## 72 Results

### 73 Learning specificity varies amongst conditioned mice.

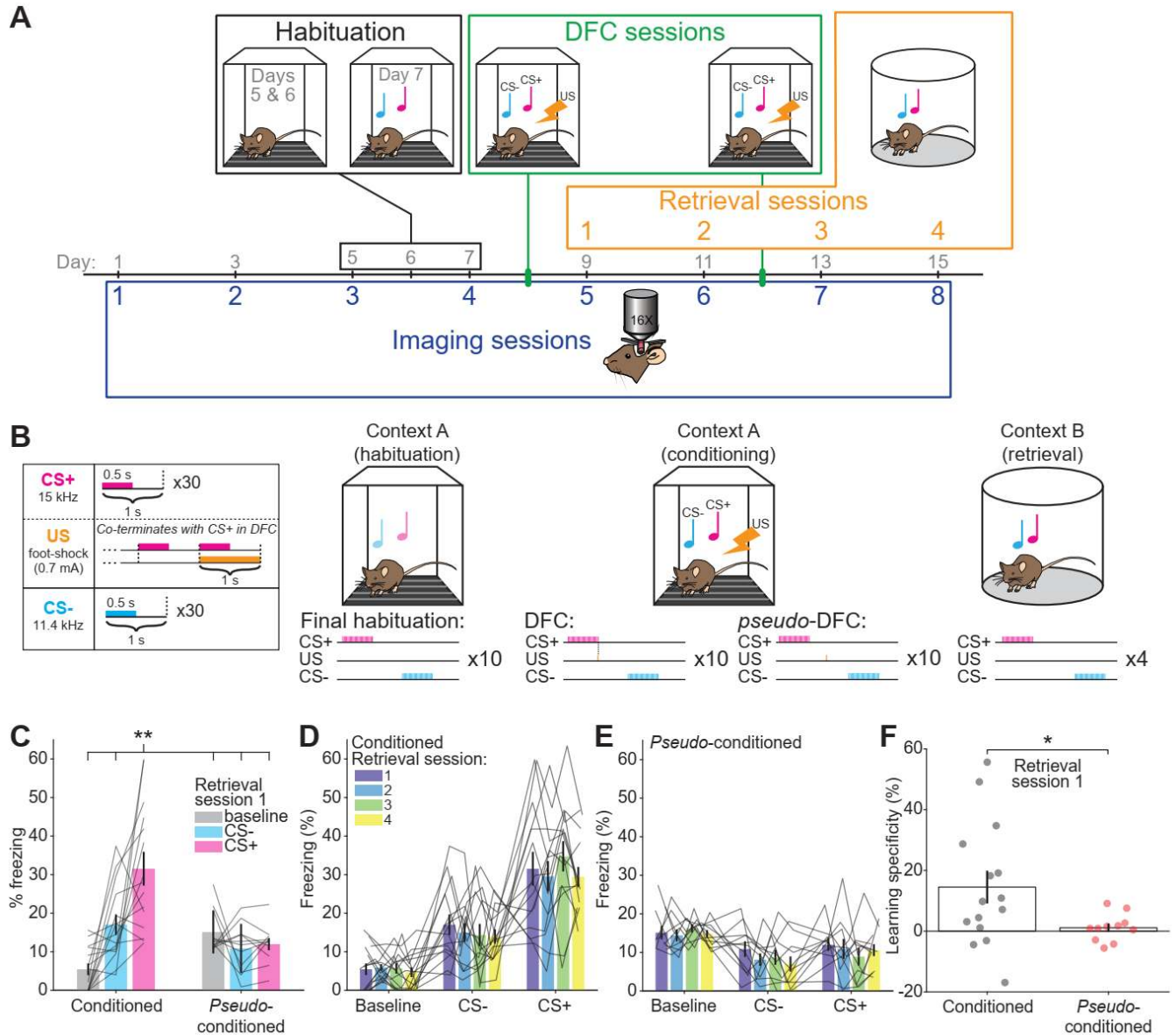
74 To establish the relationship between sound-evoked activity in the AC and differential fear  
75 conditioning, we recorded simultaneous neuronal activity from hundreds of neurons in AC. We  
76 tracked the same neurons before and after DFC, using two-photon imaging of a fluorescent  
77 calcium probe (GCaMP6<sup>20</sup>, Fig. S1-2). Longitudinal imaging of neuronal activity in large  
78 ensembles of neurons in layers 2 and 3 of AC before and after conditioning allowed us to  
79 compare the representation of the CS stimuli before and after learning (Fig. 1A).

80 Mice exhibited a range of learning specificities. We conditioned mice by exposure to 10  
81 repeats of an alternating sequence of two tones, one of which co-terminated with a foot-shock  
82 (CS+, 15 kHz), and one which did not (CS-, 11.4kHz). *Pseudo*-conditioned mice were presented  
83 with the same stimuli, but the foot-shock occurred during periods of silence between the stimuli  
84 (Fig. 1B). We measured fear-memory retrieval by presenting the same auditory stimuli to the  
85 mice in a different context and measuring the % of time the mice froze during stimulus  
86 presentation and at baseline (Fig. 1C). Following conditioning, memory retrieval was tested after  
87 each imaging session and the levels of freezing were consistent across all 4 retrieval sessions  
88 (Fig 1D-E, two-way repeated-measures (rm)-ANOVA, no effect of retrieval session on freezing,  
89  $F_{(3, 126)} = 0.91$ ,  $p = .440$ . Nor any interaction between session and stimulus type  
90 (session\*baseline/CS-/CS+,  $F_{(6,126)} = 0.70$ ,  $p = .651$ ). Similarly, freezing in *pseudo*-conditioned  
91 mice was consistent over the 4 retrieval sessions (two-way rm-ANOVA, no main of session on  
92 freezing,  $F_{(3,90)} = 0.90$ ,  $p = .442$ ; no interaction between session and stimulus type ( $F_{(6,90)} = 0.66$ ,  
93  $p = .683$ ). Since there was no change in freezing over time, we do not specifically consider  
94 results with respect to the second DFC session (Fig. 1A, day 12). Henceforth we refer to DFC  
95 as the first DFC session. Conditioned mice that did not freeze to CS+ or CS- differently from

96 baseline across all 4 retrieval sessions were excluded from subsequent analysis (6/21 mice  
97 excluded, Fig. S3A, two-way ANOVA,  $p > .05$ , see methods).

98 Learning specificity was defined as the difference between freezing to CS+ and CS- during  
99 memory retrieval sessions (see Methods, Equation 1)<sup>3</sup>. We used two pure-tone CS stimuli which  
100 have been shown to engage AC in human DFC<sup>21</sup>. The pure tones were close together in  
101 frequency space (0.40 octaves apart) in order to drive a range of learning specificities in  
102 conditioned mice that are not achievable at greater frequency distances<sup>3</sup>. Indeed, we observed  
103 that conditioned mice displayed a larger range of learning specificities (range: -16.9 to 55.6%)  
104 compared with *pseudo*-conditioned mice (-5.6 to 9.1%). This was reflected in a significantly  
105 larger standard deviation of learning specificity in conditioned mice ( $\sigma = 20.2\%$ ) than in *pseudo*-  
106 conditioned mice (Fig. 1F,  $\sigma = 4.5\%$ , *F*-test,  $F_{(14, 10)} = 20.48$ ,  $p < .001$ ) in the first retrieval session  
107 after DFC. We also observed a significantly higher learning specificity (mean: 14.5%) in  
108 conditioned mice than *pseudo*-conditioned mice (mean: 1.1%, *t*-test,  $t_{(24)} = 2.15$ ,  $p = .042$ ) in the  
109 retrieval session after DFC. Learning specificity persisted for the subsequent memory retrieval  
110 sessions over the course of the experiment in conditioned and *pseudo*-conditioned mice (Fig.  
111 S3B-D, two-way rm-ANOVA,  $p > 0.05$ , Table S1). Thus, we found that conditioned mice exhibited  
112 a range of learning specificities, with some generalizing their fear across the CS stimuli and  
113 others specializing their fear responses to CS+. On average, the learning specificity of mice was  
114 stable over the course of the experiment.

115



116 **Figure 1: Experimental timeline and differential fear conditioning (DFC) paradigm.** (A)  
 117 Experimental timeline: Mice were imaged for 4 sessions (48 hours apart) before DFC to establish  
 118 baseline responses to tone pip stimuli under the two-photon. Prior to DFC, mice were habituated  
 119 to the fear conditioning chamber. Mice were subjected to DFC (21 mice) or *pseudo*-conditioning  
 120 (11 mice) on Days 8 and 12. After DFC-1 (day 8), fear retrieval testing was performed after each  
 121 imaging session. (B) Mice were habituated to the conditioning chamber (context A) for 3 days  
 122 prior to conditioning and on the final day, the stimuli were presented without foot-shock. During  
 123 conditioning, a foot-shock (1 s, 0.7 mA) was paired with the CS+ (15 kHz, 30s pulsed at 1 Hz).  
 124 The CS- (11.4 kHz, 30 s pulsed at 1 Hz) was presented alternately with the CS+ (30-180 s apart,  
 125 10 repeats) and not paired with a foot-shock. During *pseudo*-conditioning, 10 foot-shocks were  
 126 presented randomly between the CS stimuli. During retrieval testing (context B), the same CS+  
 127 and CS- stimuli were presented alternately (30-180 s apart, 4 repeats). Motion of the mouse was  
 128 recorded and the percentage freezing during each stimulus was measured offline. (C) Freezing  
 129 at baseline (gray), for CS+ (pink) and CS- (blue) in retrieval session 1 (day 9) showing the

130 percentage of time frozen during tone presentation for CS+, CS- and baseline for each mouse.  
131 Gray lines indicate freezing for each included mouse. (\*\* Two-way ANOVA (Table S2), *Tukey-*  
132 *Kramer post-hoc* test,  $p < .01$ ). **(D)** Freezing to baseline, CS-, and CS+ for each conditioned  
133 mouse over the 4 retrieval sessions. Gray lines show each mouse. **(E)** Same as **D** for *pseudo-*  
134 conditioned mice. **(F)** Learning specificity of conditioned and *pseudo*-conditioned mice for  
135 retrieval session 1. Circles show individual mice. (\**t*-test,  $p < .05$ ). Error bars in **C-F** indicate  
136 standard error of the mean (SEM).

137

## 138 **Neuronal responses in AC pre-DFC predict specificity of fear learning.**

139 We used two-photon imaging to record calcium activity from neurons in auditory cortex in  
140 head-fixed mice (Fig. 2A). We presented 100-ms tone pips (frequency range: 5-32 kHz, including  
141 CS+ and CS- frequencies) to obtain frequency response functions from each neuron. We  
142 hypothesized that the activity in auditory cortex would predict learning specificity across  
143 individual mice. Thus, we tested whether neuronal discrimination of CS+ and CS- in AC pre-DFC  
144 predicted learning specificity following DFC. To assess how well single neurons could  
145 discriminate between the two conditioned tones, we computed the Z-score difference ( $Z_{\text{diff}}$ , see  
146 Methods, Equation 2) of responses to CS+ and CS- for responsive neurons. In an example  
147 neuron (Fig. 2B), the distributions of single-trial response magnitudes to CS+ and CS-  
148 demonstrate a separation resulting in a significant  $Z_{\text{diff}}$  score of 2.01. The  $Z_{\text{diff}}$  score of responsive  
149 neurons was considered significant if the actual score was greater than the 95<sup>th</sup> percentile of the  
150 bootstrapped  $Z_{\text{diff}}$  scores (see Methods). Figure 2C shows the distribution of  $Z_{\text{diff}}$  scores for all  
151 responsive units from conditioned mice 24 hours pre-DFC. We found that the mean significant  
152  $Z_{\text{diff}}$  scores across the 4 pre-DFC imaging sessions predicted the learning specificity 24 hours  
153 post-DFC (Fig. 2D,  $r(13) = .74$ , 95% CI [.51, .88],  $p = .002$ ). In fact, this prediction was already  
154 evident using  $Z_{\text{diff}}$  from session 4 alone (Fig. 2E,  $r(12) = .62$ , 95% confidence intervals (CI) [.00,  
155 .83],  $p = .042$ , one mouse did not have any neurons with significant  $Z_{\text{diff}}$  in this session,  
156 correlation not different from using mean  $Z_{\text{diff}}$  across all pre-DFC sessions, bootstrap  
157 comparison, see methods:  $r$  difference = 0.11, 95% CI [-0.10, 0.65],  $p = 0.316$ ,  $N = 14$ ). In  
158 summary, this suggests that the individual neuronal discriminability in AC pre-DFC predicts the  
159 learning specificity 24 hours post-DFC.

160 It is possible that the  $Z_{\text{diff}}$  score results from some underlying distributions of response  
161 magnitudes; for example, the magnitude of response to CS+ could be the driver of the prediction  
162 phenomenon. Thus, we explored whether magnitude of CS+ or CS- responses related to

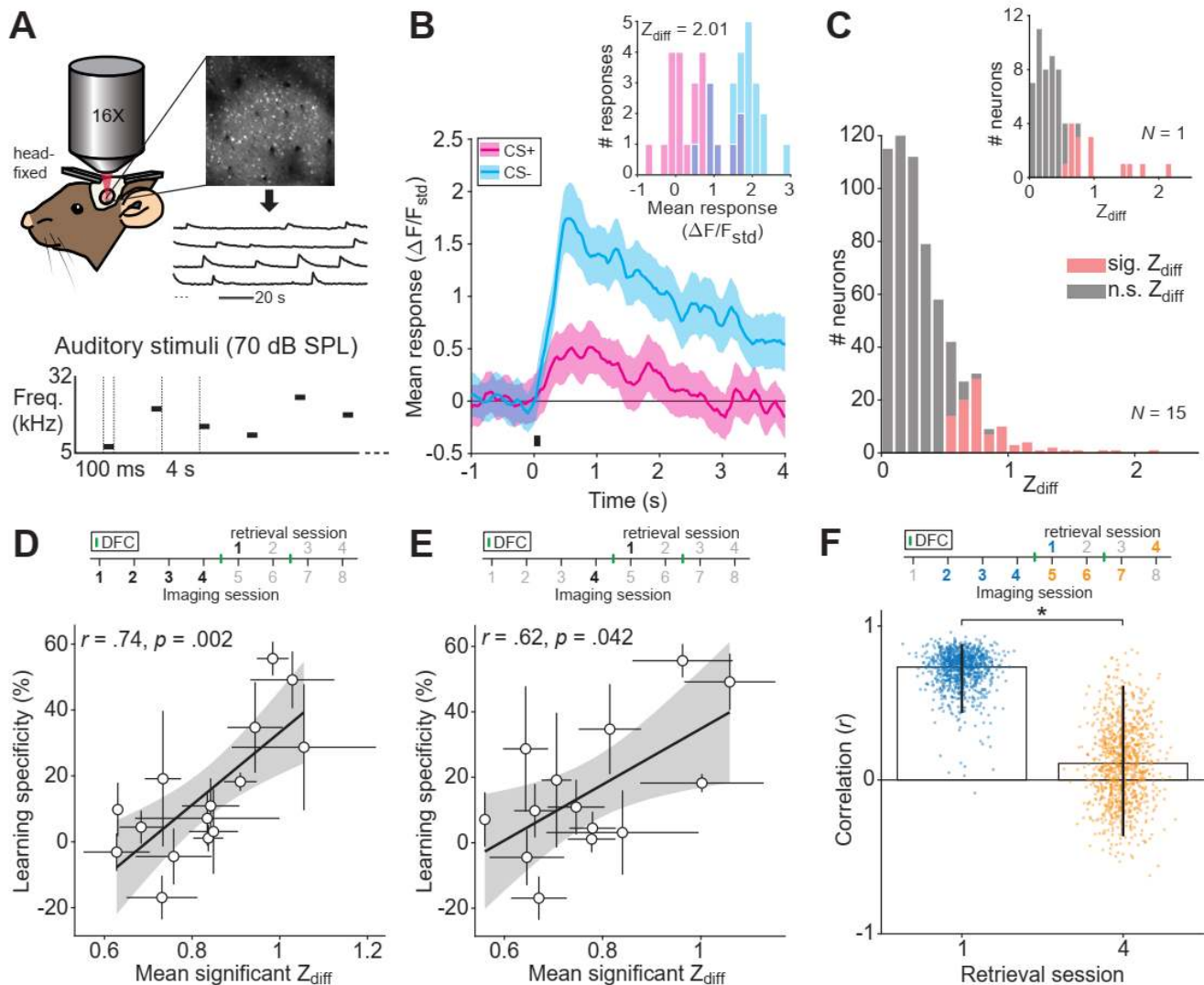


163 learning specificity. We compared the mean response magnitudes to each CS over the 4 pre-  
164 DFC imaging sessions with learning specificity 24 hours post-DFC and found that they were not  
165 correlated (Pearson's correlation,  $p < 0.05$ , Fig. S4). This suggests that it is not merely the  
166 magnitude of responses to CS+ or CS- but truly discriminability of the responses that is  
167 underlying the prediction of learning specificity.

168 We next tested the temporal window for the prediction of learning specificity. If changes in  
169 sound-evoked responses in AC reflect memory formation or the strength of learning as  
170 previously suggested<sup>15,17</sup>, we would expect a stronger relationship between the neuronal  
171 discrimination and learning specificity after DFC than before. To test this, we compared the  
172 correlations between mean  $Z_{\text{diff}}$  across equal numbers of imaging sessions (3 imaging sessions  
173 preceding retrieval sessions 1, and 4) and learning specificity before and after DFC. We found  
174 that the mean  $Z_{\text{diff}}$  score pre-DFC predicted learning specificity from retrieval session 1 ( $r(13) =$   
175  $.73$ , 95% CI  $[.43, .88]$ ,  $p = .003$ ), whereas the mean  $Z_{\text{diff}}$  score post-DFC did not predict learning  
176 specificity in retrieval session 4 ( $r(13) = .108$ , 95% CI  $[-.37, .61]$ ,  $p = .727$ ). Furthermore, the  
177 correlation pre-DFC was significantly stronger than that post-DFC (bootstrap comparison (see  
178 Methods):  $r$  difference =  $0.626$ , 95% CI  $[0.04, 1.14]$ ,  $p = .036$ ).

179 In summary, individual neuronal discriminability in AC pre-DFC predicted learning specificity  
180 24 hours after DFC. Post-DFC, neuronal activity no longer predicted learning specificity.  
181 Therefore, the role of auditory cortex in DFC is likely restricted temporally. To further investigate  
182 the relationship between neuronal and behavioral discriminability, we examined whether  
183 neuronal population discriminability could predict learning specificity.

184



185 **Figure 2: Mean neuronal discriminability pre-DFC predicts learning specificity.** (A)  
 186 Imaging setup: Mice were head-fixed under the two-photon microscope, fluorescence of calcium  
 187 indicator (GCaMP6s/m) was measured at ~30 Hz, regions of interest and mean fluorescence  
 188 over time were extracted using open software<sup>22</sup>. Schematic showing auditory stimuli, comprised  
 189 of pure-tone pips (100 ms, 70 dB SPL, 5-32 kHz) presented at 0.24 Hz. (B) Response (mean  $\pm$   
 190 SEM, 25 repeats) to the presentation (black bar) of CS+ (magenta) and CS- (cyan) of an example  
 191 neuron. Inset shows distributions of the single-trial mean responses (mean  $\Delta F/F_{std}$  across 2-s  
 192 window following stimulus onset) to CS+ and CS- from the same neuron. (C) Distribution of  $Z_{diff}$   
 193 scores of responsive units from conditioned mice 24 hours pre-DFC. Significant scores are  
 194 indicated in red,  $N = 94/617$  neurons. Inset, single mouse example,  $N = 15/62$  neurons. (D) Mean  
 195  $Z_{diff}$  score of significant- $Z_{diff}$  neurons for each mouse 24 hours pre-DFC (imaging session 4)  
 196 does not correlate with learning specificity 24 hours post-DFC (retrieval session 1). Error bars = SEM;  
 197 black line = linear regression between the mean  $Z_{diff}$  and learning specificity, gray shading = 95%  
 198 CI of the fit. (E) Mean  $Z_{diff}$  score of significant- $Z_{diff}$  neurons pre-DFC (imaging sessions 1-4)  
 199 correlated with learning specificity 24 hours post-DFC. (F) Pearson's correlation ( $r \pm 95\%$  CI)  
 200 between  $Z_{diff}$  score averaged across 3 imaging sessions preceding retrieval sessions 1 (blue),

201 and 4 (orange). Dots represent individual bootstrapped ( $n = 1000$ ) correlation values. \*  $p < 0.05$ ,  
202 bootstrap comparison, see methods.

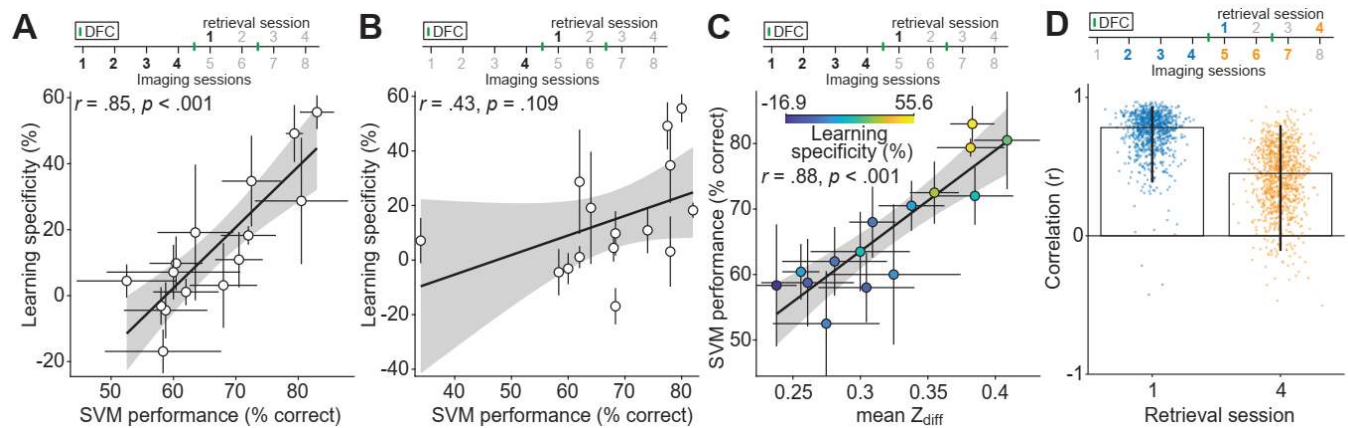
### 203 **Population neuronal activity in AC pre-DFC predicts specificity of fear learning.**

204 For many brain regions and tasks, activity of multiple neurons can provide more information  
205 in combination than averaged activity of individual neurons<sup>23–25</sup>. Using machine learning, we  
206 investigated whether populations of neurons predicted learning specificity better than the  
207 average  $Z_{\text{diff}}$  scores. We trained a Support Vector Machine (SVM) to discriminate between  
208 presentation of CS+ and CS- using population responses to the two stimuli. Mean SVM  
209 performance prior to DFC correlated with learning specificity 24 hours post-DFC (Fig. 3A,  $r(13)$   
210 = .85, 95% CI [.66, .94],  $p < .001$ ). However, unlike with the mean  $Z_{\text{diff}}$ , SVM performance 24  
211 hours pre-DFC did not predict learning specificity 24 hours post-DFC (Fig. 3B,  $r(13) = .43$ , 95%  
212 CI [.05, .76],  $p = .109$ ); significantly weaker than that of all pre-DFC imaging sessions (bootstrap  
213 comparison (see Methods),  $r$  difference = -0.42, 95% CI [-0.71, -0.13],  $p = .004$ ), potentially due  
214 to the SVM including neurons with non-specific responses that likely differed across imaging  
215 sessions. Nonetheless,  $Z_{\text{diff}}$  scores and the SVM performance of the same neurons were strongly  
216 correlated (Fig. 3C,  $r(13) = .88$ , 95% CI [.77, .95],  $p < 0.001$ ), suggesting that the two different  
217 discriminability methods used similar underlying features to discriminate the stimuli. This was  
218 also reflected in the fact that the correlations between the two discriminability measures across  
219 pre-DFC imaging sessions and learning specificity were not statistically different (bootstrap  
220 comparison,  $r$  difference = -0.11, 95% CI [-0.25, 0.01],  $p = .078$ ). Thus, population responses  
221 pre-DFC predicted subsequent learning specificity likely through similar mechanisms to the  
222 mean  $Z_{\text{diff}}$ .

223 We next tested whether predictability of learning specificity persisted after DFC by  
224 comparing the mean SVM performance across the 3 preceding imaging sessions with retrieval  
225 sessions 1 and 4 (Fig. 3D). The mean SVM performance pre-DFC (predicted learning specificity  
226 in retrieval session 1 ( $r(13) = .78$ , 95% CI [.38, .94],  $p < .001$ ). However, the mean SVM  
227 performance post-DFC did not predict learning specificity in retrieval session 4 ( $r(13) = .46$ , 95%  
228 CI [-.11, .80],  $p = .092$ ). However, the two correlations were not significantly different (bootstrap  
229 comparison,  $r$  difference = 0.331, 95% CI [-0.12, 0.90],  $p = .150$ ). Combined with similar results  
230 from the mean  $Z_{\text{diff}}$  scores (Fig. 2F), there is some evidence to support that neuronal  
231 discriminability before conditioning predicts learning specificity but no longer predicts learning

232 specificity after conditioning. This suggests that neuronal discrimination in the output layers of  
 233 AC is involved in the initial discrimination during, but not after, differential fear conditioning.

234



235 **Figure 3: Neuronal population discrimination between CS+ and CS- pre-DFC predicts**  
 236 **learning specificity.** (A) SVM performance 24 hours pre-DFC (imaging session 4) does not  
 237 predict learning specificity 24 hours post-DFC (retrieval session 1,  $N = 15$ ). (B) SVM  
 238 performance (Mean  $\pm$  SEM) across pre-DFC sessions (imaging sessions 1-4) predicts learning  
 239 specificity 24 hours post-DFC (retrieval session 1). (C) Mean ( $\pm$  SEM) SVM performance pre-  
 240 DFC correlates with the mean ( $\pm$  SEM)  $Z_{diff}$  score pre-DFC (imaging sessions 1-4). Fill color  
 241 indicates learning specificity from retrieval session 1. (D) Correlation ( $r \pm 95\%$  CI) between SVM  
 242 performance averaged across 3 imaging sessions preceding retrieval sessions 1 (blue), and 4  
 243 (orange). Dots represent individual bootstrapped correlation values ( $n = 1000$ ). Black lines in A,  
 244 B, & C show the linear fit between the two variables, shading = 95% CI. Circles represent  
 245 individual mice with error bars = SEM. Statistics in A-D: Pearson's correlation.

246 **After DFC, discriminability between CS+ and CS- is preserved in conditioned mice.**

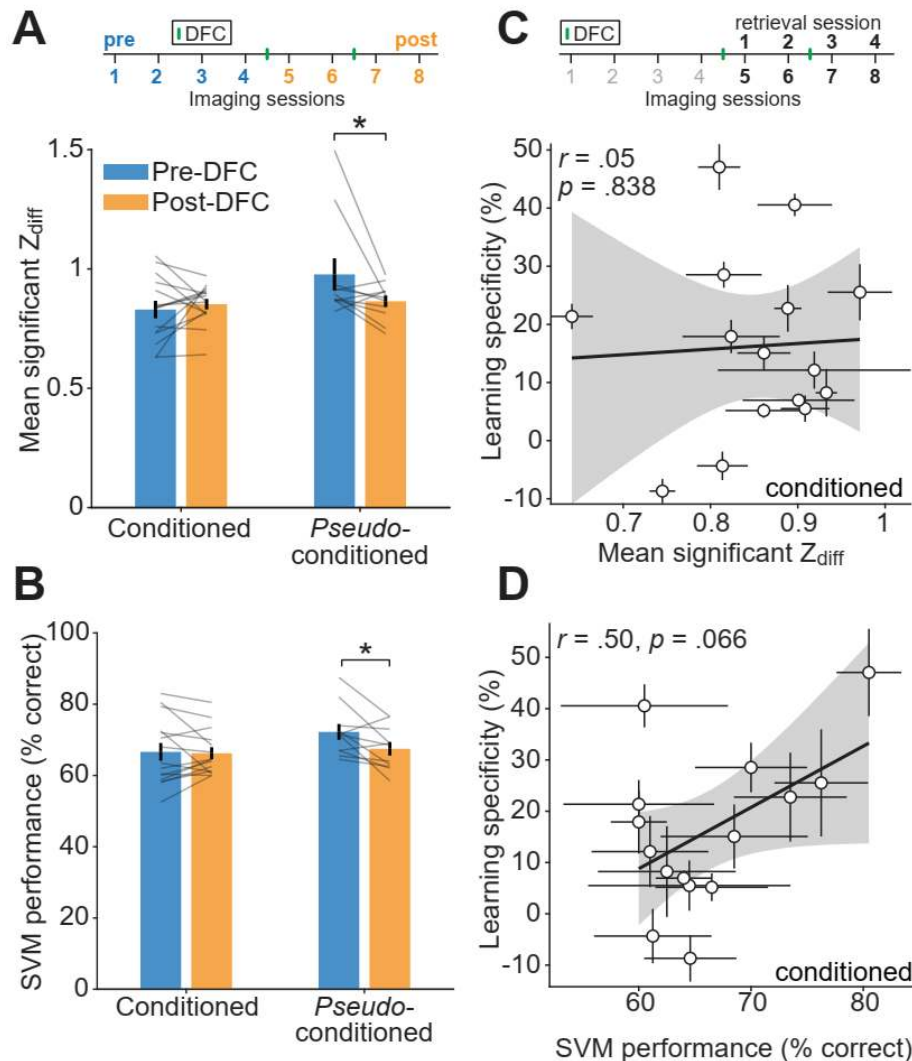
247 It has been suggested that 'fear memories' are encoded in the auditory cortex following  
 248 differential fear conditioning<sup>15,17</sup>, such that neuronal discriminability may improve following  
 249 conditioning. We found that neuronal activity following DFC no longer predicted learning  
 250 specificity (Fig. 2F, 3D), suggesting AC does not support the fear response after DFC. We tested  
 251 whether the neuronal discriminability of CS+ and CS- changed after DFC by comparing the mean  
 252  $Z_{diff}$  across pre- and post-DFC sessions (Fig. 4A, rm-ANOVA, Table S3). We found no change in  
 253  $Z_{diff}$  from pre- to post-DFC in conditioned mice ( $p = .581$ ), whereas there was a significant  
 254 decrease in *pseudo*-conditioned mice ( $-0.11 \pm 0.05$  units, *Tukey-Kramer post-hoc* comparison,  
 255  $p = .026$ ). Results were similar at a neuronal population level; mean SVM performance in  
 256 conditioned mice did not change across pre- and post-DFC sessions (Fig. 4B, rm-ANOVA, Table  
 257 S4, *Tukey-Kramer post-hoc* comparison,  $p = .802$ ), whereas there was a significant decrease in  
 258 *pseudo*-conditioned mice ( $-4.7 \pm 1.8\%$ , *Tukey-Kramer post-hoc* comparison,  $p = .014$ ).

259 Combined, we found that following DFC or *pseudo*-conditioning, neuronal discrimination  
260 between the CS+ and CS- was maintained in conditioned mice, while it decreased in *pseudo*-  
261 conditioned mice. These results suggest that AC does not store fear memory by increasing  
262 discriminability. Rather, plasticity in AC appears to counteract previously reported habituation in  
263 neuronal responses to repeated stimuli<sup>18,26</sup>.

264 To further investigate whether the changes in stimulus representation were related to DFC,  
265 we tested the neuronal discrimination performance of the SVM on each imaging session using  
266 cells tracked across consecutive imaging sessions. We trained the SVM using the first session  
267 ( $n$ ) and tested on data held out from that session and from the following session ( $n + 1$ ). If  
268 reorganization of stimulus representation between days contributes to stimulus discrimination,  
269 we would expect a change in performance following DFC. We did not observe any consistent  
270 changes in SVM performance following DFC in conditioned or *pseudo*-conditioned mice (Fig.  
271 S5A, two-way rm-ANOVA with dependent variable; SVM performance and independent  
272 variables; session comparison (1 & 2, 2 & 3... to 7 & 8) and conditioning type (DFC/*pseudo*-  
273 conditioning, no effect of)  $p > 0.05$  for session and interaction, Table S5). Similarly, we did not  
274 observe any significant changes in mean  $Z_{\text{diff}}$  in neurons tracked between any of the consecutive  
275 sessions of the experiment (Fig. S5B, Table S6). Overall, these results indicate that changes  
276 that occurred in stimulus representation do not contribute to the neuronal stimulus discrimination  
277 in fear memory retrieval.

278 Different levels of learning specificity across mice could potentially account for the different  
279 levels of neuronal discriminability post-DFC. We therefore tested whether there was any  
280 correlation between the neuronal discriminability (mean  $Z_{\text{diff}}$  score and SVM performance) and  
281 the learning specificity *post*-DFC. The mean  $Z_{\text{diff}}$  score (imaging sessions 5-8) did not correlate  
282 with the mean learning specificity of conditioned mice across the 4 *post*-DFC sessions (Fig. 4C,  
283 Pearson's correlation,  $r(13) = .05$ , CI [-.45, .56],  $p = .838$ ), nor was there a correlation between  
284 the mean SVM performance *post*-DFC and the mean learning specificity *post*-DFC (Fig. 4D,  
285  $r(13) = .49$ , CI [-.19, .86],  $p = .066$ ). This suggests that neuronal discriminability *post*-DFC does  
286 not reflect learning specificity.

287



288 **Figure 4: Changes in stimulus information representation post-DFC.** (A) Comparison  
 289 of mean  $\pm$  SEM significant- $Z_{diff}$  between the pre- (sessions 1-4, blue) and post-DFC sessions (5-  
 290 8, orange) in conditioned and *pseudo*-conditioned mice. Stats: *Tukey-Kramer post-hoc*:  $*p < .05$ ,  
 291 Table S3. (B) Same as A but for comparison of mean  $\pm$  SEM SVM performance between the pre- and post-DFC.  
 292 Stats: *Tukey-Kramer post-hoc*:  $*p < .05$ , Table S4. (C) Relationship between  
 293 mean significant- $Z_{diff}$  across the post-DFC sessions (sessions 5-8) and mean learning specificity  
 294 across the same sessions. Statistics: Pearson's correlation. Black line shows linear fit (shading  
 295 = 95% CI of the fit). (D) Same as C but for mean SVM performance across the post-DFC  
 296 sessions (sessions 5-8) and mean learning specificity across the same sessions. Statistics:  
 297 Pearson's correlation.

298

299 **After DFC, normalized responses at CS+ increased in conditioned mice.**

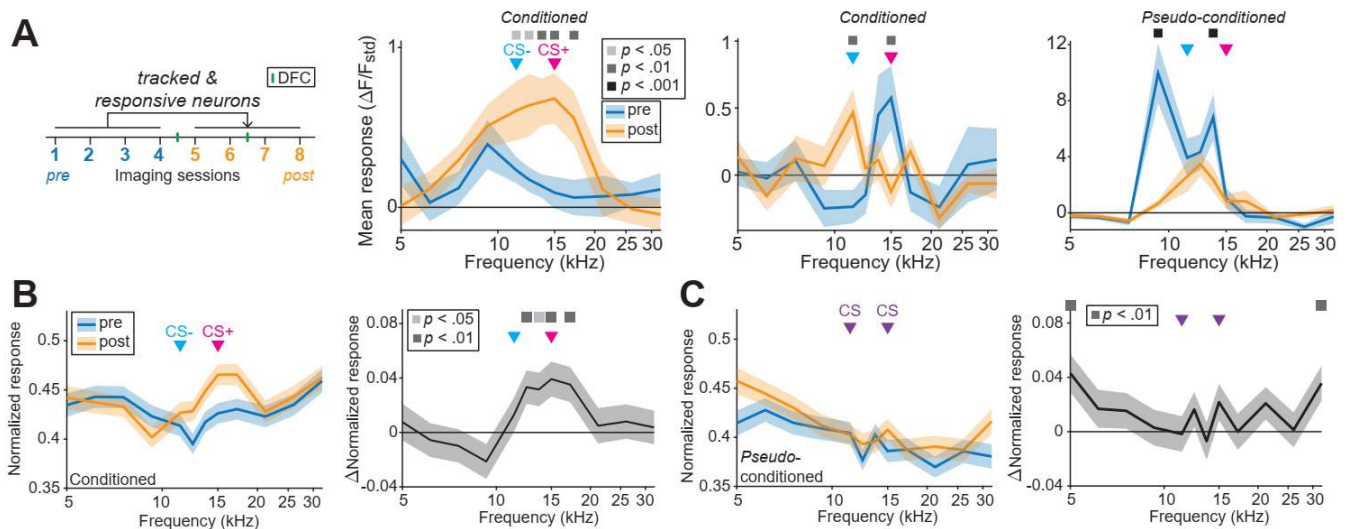
300 It has previously been shown that after differential conditioning with pure tones, select  
 301 neurons in AC amplified the difference between CS+ and CS-<sup>17,27</sup>. However, since we observed

13

302 no change in neuronal discrimination in conditioned mice, we hypothesized that there would be  
303 no change in response to CS+ and CS-. To test whether responses were altered by conditioning,  
304 we compared frequency response functions from the pre- and post-DFC imaging sessions of  
305 responsive neurons that were tracked from pre- to post-DFC (Fig. S6A). On an individual neuron  
306 basis, we observed heterogeneous changes in the frequency tuning (Fig. 5A, Table S7-9).  
307 However, we found that, on average, in conditioned mice, the *normalized* response to CS+ and  
308 frequencies between the CS+ and CS- increased, whereas the response at CS- did not change  
309 (Fig. 5B, two-way rm-ANOVA, *Tukey-Kramer post-hoc* testing,  $p < .05$ , Table S10). In contrast,  
310 in *pseudo*-conditioned mice, the mean normalized responses at most frequencies, including both  
311 CS frequencies, did not change (Fig. 5C, Table S11). When comparing responses at CS- and  
312 CS+ in conditioned mice and the CS stimuli combined (CSc) in *pseudo*-conditioned mice, we  
313 found that there was a significant increase at the CS+ and no change at CS- or CSc (Table S12,  
314 *Tukey-Kramer post-hoc* comparison,  $p = .002$ ). Although we observed an increase in normalized  
315 response to CS+, we did not observe any significant changes in non-normalized response to  
316 conditioned frequencies in conditioned mice (Fig. S6B, D, & E, Table S13-15) and we observed  
317 decreased responses to most frequencies in *pseudo*-conditioned mice (Fig. S6C, F, & G, Table  
318 S16-18). When comparing non-normalized response changes to CS+, CS- and CSc, we found  
319 a significant decrease at CSc but not at CS+ or CS- (Table S19, *Tukey-Kramer post-hoc*  
320 comparison,  $p < .001$ ). It is possible that the normalization of the frequency response functions  
321 has amplified a small change that is not strong enough to present in the absolute responses.

322 Despite the lack of significant change in the absolute responses, it is possible that the  
323 increase in normalized responses at CS+ and the lack of change in response at CS- in  
324 conditioned mice could lead to improved discriminability between CS+ and CS- by increasing  
325 the difference between the responses to each stimulus. This would be consistent with the  
326 hypothesis that, following fear conditioning, reorganization of neuronal activity serves to amplify  
327 the *relative* difference in responses to CS+ and CS- thereby supporting discriminability<sup>17,19</sup>.  
328 However, when we compared the magnitude of changes in normalized response to CS+, CS-,  
329 and the difference between the two with learning specificity, we did not find any correlation (Fig.  
330 S7), suggesting that the changes observed are in fact not related to storage of the fear memory  
331<sup>28</sup>. We further investigated by checking for a relationship between the *change* in neuronal  
332 discrimination ( $Z_{diff}$  & SVM performance) and learning specificity (Fig. S8) finding negative

333 correlations between the two factors. This possibly supports the idea that cortical activity is  
 334 reorganized following DFC in a way that does not support this form of fear memory.  
 335



336 **Figure 5: Changes in frequency representation post-DFC. (A)** We tracked the responses  
 337 of the same responsive neurons pre- and post-DFC. The right panels show three example  
 338 frequency response functions from tracked neurons from conditioned and *pseudo*-conditioned  
 339 mice pre-DFC (blue) and post-DFC (orange). Significant differences in the response functions  
 340 are indicated by the squares above (paired *t*-test, FDR-corrected for multiple comparisons – see  
 341 methods). The two arrows show the frequencies of the CS- (11.4 kHz) and CS+ (15 kHz) and  
 342 CSc. Two-way rm-ANOVA, *Tukey-Kramer post-hoc* analysis (Table S7-9). **(B)** (left panel) Mean  
 343 normalized frequency response functions of responsive neurons that were tracked pre- to post-  
 344 DFC across all conditioned mice ( $N = 15$  mice,  $N = 826$  neurons). (right panel) Mean change  
 345 in normalized frequency response functions of the same neurons, squares indicate significant  
 346 changes (Two-way rm-ANOVA, *Tukey-Kramer post-hoc* analysis, Table S10). **(C)** (left panel)  
 347 Mean normalized frequency response functions of responsive neurons tracked pre- to post-DFC  
 348 across all *pseudo*-conditioned mice ( $N = 11$  mice,  $N = 712$  neurons). (right panel) Mean change  
 349 in normalized frequency response functions for the same cells, square indicate significant  
 350 changes (Two-way rm-ANOVA, *Tukey-Kramer post-hoc* analysis, Table S11).

351

352 Previous studies found that the best frequency of neurons shifts towards the conditioned  
 353 stimulus (CS+) after DFC with pure tones<sup>17</sup>. We found no difference in best frequency changes  
 354 between conditioned and *pseudo*-conditioned mice (Fig. 6A & B, two-way rm ANOVA, *Tukey*-  
 355 *Kramer post-hoc* comparisons,  $p = .905$ , Table S20). However, consistent with a shift in best  
 356 frequency towards the CS+, we did observe a small decrease in the absolute distance of best  
 357 frequency from CS+ (of mean response functions pre- and post-DFC for each neuron) in  
 358 responsive neurons of conditioned mice (Fig. 6C, -0.06 octaves, two-way rm ANOVA, *Tukey*  
 359 *Kramer post-hoc*,  $p = .002$ , Table S21) but not in *pseudo*-conditioned mice ( $p = .969$ ). It is

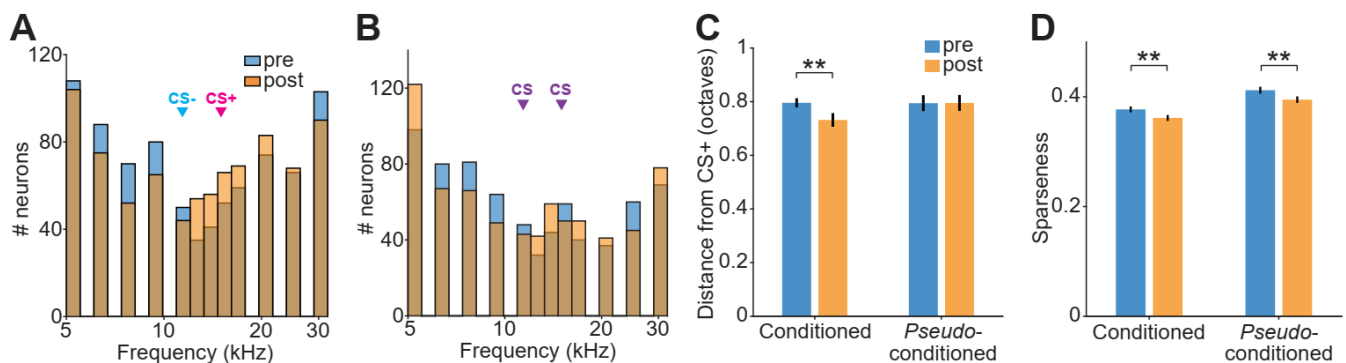


360 possible that neuronal discrimination between CS+ and CS- could be altered by a change  
361 frequency tuning width<sup>12</sup>. As a measure of tuning width we used the sparseness of the frequency  
362 response function<sup>29,30</sup>: A neuron with high sparseness responds strongly to one or few  
363 frequencies tested and little to other frequencies. A neuron with a sparseness of zero would  
364 indicate an equal response to all frequencies tested. We found no difference between the  
365 conditioned and *pseudo*-conditioned mice (Fig. 6D, two-way rm-ANOVA, *Tukey-Kramer post-hoc*  
366 comparison  $F_{(1,1883)} = 0.26$ ,  $p = .610$ , Table S22) and that sparseness decreased in both ( $F_{(1,1883)}$   
367  $= 18.25$ ,  $p < .001$ ).

368 In summary, we observed heterogeneous changes in responses of individual neurons  
369 tracked from pre- to post-DFC. In conditioned animals, there was, on average, an increase in  
370 normalized response at CS+ and no change at CS-, however increase was not observed in  
371 absolute response changes. In *pseudo*-conditioned mice, we observed no changes in  
372 normalized responses at the CS stimuli. We observed a small shift in best frequency towards  
373 CS+ in conditioned mice. Sparseness of the response functions decreased in both conditioned  
374 and *pseudo*-conditioned mice, indicating that frequency tuning became broader after  
375 conditioning, thus unlikely to support increased discriminability. Combined, these results  
376 reconcile our findings with previous studies, which had effectively, by not sampling responses  
377 from the same neurons pre- and post-DFC, normalized the responses. It is plausible that  
378 previous studies observed an increase in normalized activity, which did not translate into an  
379 actual population-wide increase in discriminability as we find here.

380

381



382 **Figure 6: Best frequency and tuning sparseness pre- and post-conditioning. (A)**  
383 **Distributions of best frequencies of responsive neurons pre- (blue) and post-conditioning**  
384 **(orange),  $N = 826$ . (B) Same as A for *pseudo*-conditioned mice,  $N = 712$ . (C) Distance of best**  
385 **frequency from CS+ (15 kHz) of neurons from conditioned and *pseudo*-conditioned mice pre-**

386 (blue) and post-conditioning (orange). Stats: 2-way ANOVA *Tukey-Kramer post-hoc* analysis  
387 (Table S21). **(D)** Sparseness of mean frequency response functions of neurons from conditioned  
388 and pseudo-conditioned mice pre- (blue) and post-conditioning (orange). Statistics: 2-way  
389 ANOVA *Tukey-Kramer post-hoc* analysis (Table S22). \*\*  $p < .01$ . Error bars = SEM.

390

## 391 **A learning model of the fear circuit**

392 We found that AC activity prior to learning predicts specificity of learning, yet the reorganized  
393 neuronal responses do not correlate with learning specificity. In order to better understand our  
394 findings in relation with previous results, we built a simple model that consisted of two frequency-  
395 tuned populations of neurons and a neuronal population that responds to the foot-shock. Our  
396 goal was to test whether this simple model could account for both the findings in this manuscript  
397 and from previous work, in particular: (1) Discriminability between CS+ and CS- in AC predicts  
398 learning specificity post-DFC (Fig. 2-3); (2) Suppressing inhibition in AC leads to increased  
399 generalization (decreased learning specificity) post-DFC <sup>12</sup>; (3) Suppressing AC post-DFC does  
400 not affect learning specificity <sup>3,11</sup>.

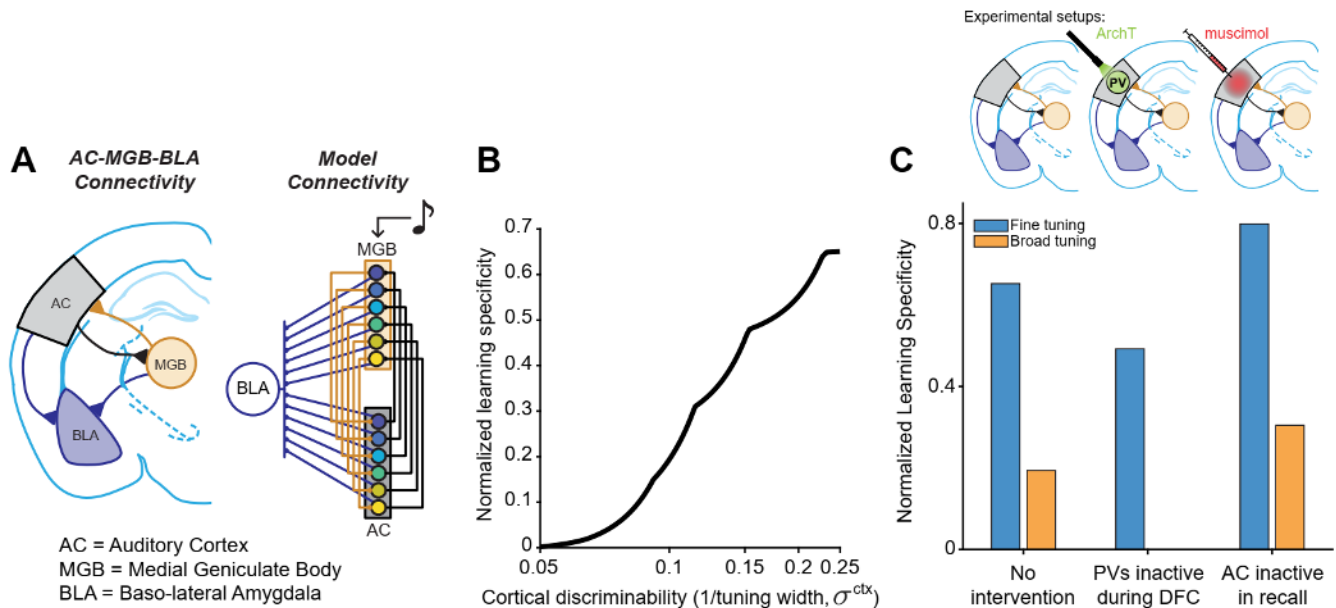
401 In the model, we included two populations of frequency-tuned neurons (representing the  
402 medial geniculate body, MGB, and AC). MGB receives auditory inputs and projects to AC. Both  
403 populations project to basolateral amygdala (BLA). AC sends tonotopically organized feedback  
404 connections to MGB. During conditioning, the MGB neurons receive sound inputs and the  
405 neurons in the BLA are active during the foot-shock (Fig. 7A). The weights from MGB and AC to  
406 BLA are updated according to a Delta learning rule (see Methods), that is, they are potentiated  
407 when both are co-activated (i.e. when the foot-shock coincides with the sound stimulus). We  
408 control the level of overlap in frequency tuning between neurons in AC and use it to represent  
409 frequency discriminability (more overlap = less discriminability). The activity of the BLA after  
410 weight update and with auditory input only is used as a measure of freezing.

411 We first tested whether broad tuning in AC (low neuronal discriminability between CS+  
412 and CS-) produced more generalized freezing than sharp tuning (high neuronal discriminability).  
413 We found that increased overlap in frequency tuning in AC neurons, without changing the tuning  
414 of MGB neurons, drove more generalized freezing responses (Fig. 7B, S9). This is due to the  
415 fact that, when AC was broadly tuned, CS+ tone activated AC neurons not only responded to  
416 the CS+ frequency but also to other frequencies, such as the CS-, albeit to a lesser extent. After  
417 learning, this resulted in strong AC to BLA synaptic weights that are not specific to CS+. MGB

418 is narrowly tuned in our model, but the weights from MGB to BLA were also strengthened in a non-  
 419 specific fashion (Fig. S9) because AC projects back to MGB. Therefore, CS+ also activated non-  
 420 specific neurons in MGB concurrently with the foot-shock. These results support the present  
 421 findings (Fig. 2, 3). Second, we examined the effects of decreasing inhibition in the AC population  
 422 during conditioning (Fig. 7C, S10). Decreasing inhibition resulted in an increased overlap in  
 423 frequency responses in the AC population, which in turn led to increased generalization,  
 424 supporting previous findings and providing a mechanism<sup>12,31</sup>. Third, we tested whether  
 425 inactivating the auditory cortex following conditioning had an effect on freezing responses (Fig.  
 426 7C, S11). Consistent with previous findings<sup>3,11</sup>, we did not observe a change in fear  
 427 generalization following AC inactivation. The broad or narrow tuning of AC neurons allowed for  
 428 the synapses from MGB to BLA to be strengthened either narrowly or broadly during  
 429 conditioning. Therefore, with suppression of AC during memory recall, the specialized versus  
 430 generalized learning was preserved.

431 Combined, the model demonstrates that a simple anatomically consistent circuit supports  
 432 multiple aspects of cortical control of fear conditioning identified here and in previous studies.

433



434 **Figure 7: A learning model reconciles present and past findings. (A)** (left panel)  
 435 connectivity between auditory cortex (AC, gray), medial geniculate body (MGB, orange) and  
 436 basolateral amygdala (BLA, blue). Right panel shows the model connectivity. MGB receives  
 437 auditory input and provides input to AC (orange lines), and both MGB and AC provide inputs to  
 438 BLA (blue lines). AC feeds back to MGB (black lines). Colored circles represent neurons tuned to  
 439 different, overlapping frequency ranges. **(B)** Normalized learning specificity output from the  
 440 model with varying levels of AC discriminability, achieved by changing the frequency tuning

441 overlap between the neurons in the AC population,  $\sigma^{ctx}$ . **(C)** Normalized learning specificity at  
442 two AC discriminability levels; fine (blue) and broad (orange) tuning. Results are shown for  
443 learning specificity with no interventions, when inhibition is reduced in AC during DFC (analogue  
444 of when ArchT-transfected PV interneurons in AC are inactivated by optogenetics during DFC),  
445 and when AC is inactivated during memory recall (analogue of an injection of muscimol during  
446 memory recall; PV = parvalbumin positive interneurons, ArchT = Archaeorhodopsin-T).

## 447 Discussion

448 Our results identify the role of the auditory cortex in differential fear learning: (1) Prior to fear  
449 learning, neuronal responses in AC shape fear learning specificity (Fig. 2 & 3); (2) Following  
450 differential fear conditioning, neuronal response transformations are not correlated with fear  
451 learning specificity (Fig. 5, Fig. S7), and therefore the auditory cortex does not encode auditory  
452 differential fear memory; (3) Neuronal activity in AC post-DFC does not correlate with freezing  
453 behavior (Fig. 4); (4) A simple model of the auditory nuclei and the basolateral amygdala could  
454 account for our results as well as a number of previous findings (Fig. 7).

455 Our finding that the neuronal activity prior to fear conditioning predicted specialization of fear  
456 learning provides a mechanism for the role of AC in differential fear memory acquisition<sup>10–12,14,31</sup>.  
457 Specifically, inactivation of inhibitory neurons in the AC during fear conditioning led to increased  
458 generalization of fear learning with pure tones<sup>12</sup>. Suppressing inhibitory neurons in the AC led  
459 to a decrease in Fisher information, which reflects the certainty about a stimulus in neuronal  
460 representation<sup>31</sup>. This change would likely result in a decrease in neuronal discriminability  
461 between the dangerous and safe tones in the AC, and therefore drive an increase in fear  
462 generalization, as demonstrated by our model (Fig. 7). Our results provide the link between  
463 optogenetic inactivation of interneurons in AC leading to increased fear generalization, and to  
464 increased frequency tuning width<sup>12</sup>, which decreases neuronal discriminability.

465 By using two-photon imaging to record from the same neurons over the course of differential  
466 fear conditioning, we were able to compute changes in both absolute and relative neuronal  
467 activity of a large number of identified neurons, a feat not normally achievable with  
468 electrophysiology<sup>17,19</sup>. Previous work found that changes in neuronal responses to the  
469 dangerous and safe stimuli after differential fear conditioning amplified the difference between  
470 the responses<sup>17,19</sup>. This change was proposed to represent fear memory<sup>15,19,28</sup>. We identified  
471 similar transformations in the *normalized* response functions of neurons that were tracked pre-  
472 to post-conditioning, we found an increased relative response to the CS+. However, these  
473 changes did not correlate with freezing behavior suggesting that the neuronal code in the AC

474 after fear conditioning does not reflect differential fear memory. Indeed, a number of studies  
475 found that inactivating the auditory cortex *after* fear conditioning with pure tones does not affect  
476 fear memory retrieval<sup>3,11</sup> (but see<sup>14</sup>). Combined, our results restrict the role of auditory cortex  
477 in fear conditioning to pure tone differential fear memory acquisition, but not retrieval.

478 If the increase in normalized response at CS+ is not related to fear memory, then why is  
479 there an increase in response? It could be reflective of increased attention caused by  
480 presentation of the CS+ and that the discrimination of the CS stimuli is unaffected by this effect  
481<sup>32</sup>. Furthermore, changes in frequency map organization do not necessarily relate to changes in  
482 behavioral frequency discrimination of pure tones<sup>33,34</sup>, thus over-representation of the CS+ could  
483 be induced by learning but not necessary for discrimination learning.

484 To locate our findings with previous work, we implemented a simple, anatomically  
485 accurate<sup>35,36</sup> model with connections from auditory nuclei to the basolateral amygdala (Fig. 7).  
486 The model demonstrated that (1) neuronal activity in cortex can predict subsequent learning  
487 specificity; that (2) inactivation of PV interneurons in AC during DFC leads to increased  
488 generalization<sup>12</sup>, and that (3) the auditory cortex is not necessary for differential fear memory  
489 retrieval<sup>3,11</sup>. The model proposes that either MGB or AC or a combination of both can induce  
490 auditory fear memory through the strengthening of connections in the amygdala. We propose  
491 that feedback from auditory cortex to the MGB contributes to discrimination of perceptually  
492 similar pure tone stimuli during DFC by controlling stimulus discrimination in the MGB, this may  
493 or may not be a direct projection neuroanatomically<sup>35,37,38</sup>. Future studies need to explore the  
494 role of the MGB and specific projections between AC, MGB and BLA in fear learning and  
495 memory. It is likely that such an important behavioral modification as fear has redundant  
496 pathways to obtain the same behavioral outcomes<sup>11,39-41</sup>.

497 Our results relied on tracking the neuronal responses in all transfected neurons in AC without  
498 distinguishing between different neuronal subtypes. Previous studies found that a specific class  
499 of inhibitory neuron increases activity with presentation of repeated tones<sup>18,26</sup>. It is therefore  
500 plausible that our results include a subset of neurons that function differently during fear  
501 conditioning but which we are unable to identify due to lack of selective labelling. Furthermore,  
502 we restricted our recordings to layers 2 and 3 of the auditory cortex, and it is possible our results  
503 overlook more specific changes in the thalamo-recipient layers of the cortex<sup>42,43</sup>. We imaged  
504 neuronal activity in layers 2/3 because those are the output layers of the cortex, and therefore  
505 the plastic changes that occur within the cortex should be evident in these layers. The complexity

506 of transformations in the cortical microcircuit and between layers with learning can be explored  
507 further <sup>44–46</sup>.

508 The results of the study may be restricted to pure tone stimuli. We chose pure tone stimuli  
509 because these stimuli provide a well-defined axis (frequency) along which to vary stimulus  
510 discriminability. Furthermore, in human subjects, AC encodes threat during DFC for pure tone  
511 stimuli <sup>21</sup>. Our prior work has established that large frequency separation between CS+ and CS-  
512 results in uniform specificity of the fear response among subjects, whereas smaller frequency  
513 separation, such as the one used here, provides for a gradient of specificity across subjects <sup>3,12</sup>.  
514 Other studies have found that AC is not behaviorally relevant for discrimination between pure  
515 tones separated by large frequency distances <sup>11,13</sup>. However, when the frequencies were brought  
516 closer together, then manipulation of AC activity did affect behavior <sup>13</sup>. Therefore, it is unclear  
517 whether recent conclusions that AC is involved in processing of more complex stimuli and not  
518 pure tones are due to differences in complexity of the stimulus, or to the degree to which AC can  
519 discriminate these stimuli. Furthermore, the FM sweeps used in these studies are not  
520 necessarily more complex than pure-tones for AC processing. Indeed, neurons in the inferior  
521 colliculus, which is two synapses earlier than AC, differentiate between FM sweeps <sup>e.g. 47</sup>.  
522 Ultimately, the relevant aspect of the present study was the ability to measure how well neuronal  
523 ensembles differentiate between two stimuli. We achieved this by bringing CS+ and CS- close  
524 together in frequency, and we found that neuronal discriminability of the stimuli differs across  
525 mice and correlates with behavioral discriminability prior to DFC. We would not expect this result  
526 were the stimuli not relevant for AC. Future studies will dissect to what extent the differences in  
527 neuronal codes in AC shape differential fear learning of more complex and natural sounds and  
528 its role in other forms of learning <sup>13,34,48,49</sup>.

529 Our results may be applicable to understanding anxiety disorders. An extreme example of  
530 fear generalization is realized in PTSD <sup>50</sup>. Here we find that the present state of each individual  
531 brain, in terms of neuronal discrimination of stimuli, is predictive of the future generalization of  
532 fear in the subject. This suggests that a way to prevent generalization of dangerous and safe  
533 sounds is to improve neuronal discrimination of potentially threatening stimuli <sup>51–54</sup>. Further work  
534 in this area can lead to a deeper understanding how genetic and social factors, as well early life  
535 experiences, shape the role of sensory cortex in this common and devastating disorder <sup>7,53</sup>.

536 We identified a neuronal correlate for inter-individual differences in learning specificity. We  
537 found that the mammalian sensory cortex plays key role in stimulus discrimination during, but

538 not following, differential fear conditioning. These results reconcile several previous findings and  
539 suggest that the role of sensory cortex is more complex than previously thought. Investigating  
540 the changes in the cortico-amygdala circuit during fear learning will pave way for new findings  
541 on the mechanisms of learning and memory.

## 542 **Acknowledgements**

543 The authors thank Dr. Yale Cohen, Dr. Steve Eliades and Dr. Jay Gottfried on helpful  
544 discussions and comments on an earlier version of the manuscript. The authors also thank other  
545 members of the Geffen laboratory for their helpful advice. This work was supported by funding  
546 from the National Institute of Health grants R01DC015527, R01DC014479 and R01NS113241  
547 to MNG.

548

## 549 **Author Contributions**

550 Conceptualization, M.N.G. and K.C.W.; Methodology, K.C.W, M.N.G., C.F.A. and C.C.;  
551 Software, K.C.W.; Investigation, K.C.W. and K.O.; Formal Analysis, K.C.W. and M.N.G; Writing  
552 – Original Draft, K.C.W., C.C, M.N.G.; Writing – Review and Editing, K.C.W., M.N.G. and C.C.;  
553 Funding Acquisition, M.N.G.; Resources, M.N.G., K.O. and K.C.W.; Supervision, M.N.G.

## 554 **Declaration of Interests**

555 The authors declare no competing interests.

## 556 **Online methods**

### 557 **Mice**

558 All experimental procedures were in accordance with NIH guidelines and approved by the  
559 IACUC at the University of Pennsylvania. Mice were acquired from Jackson Laboratories (22  
560 male, 10 female, mean age of cranial window implant: 9.6 weeks [6.3 – 13.0 weeks]; PV-Cre (4)  
561 [Stock No: 017320], PV-Cre x ROSA (1) [Stock No: 003474], CamKII-Cre mice (1) [Stock No:  
562 005359] or Cdh-23 mice (26) [Stock No: 018399]) and were housed in a room with a reversed  
563 light cycle. Experiments were carried out during the dark period. Mice were housed individually  
564 after the cranial window implant. 21 mice (15 males, 6 females) were in the conditioning group  
565 and 11 mice (7 males, 4 females) were in the *pseudo*-conditioning control group.

566 The Auditory Brainstem Response (ABR) to broadband clicks (2 – 80 kHz, 70 dB SPL) was  
567 acquired before or at the end of the experiment when possible in order to confirm that the mice  
568 had good hearing (Fig. S12).

569 Euthanasia procedures were consistent with the recommendations of the American  
570 Veterinary Medical Association (AVMA) Guidelines on Euthanasia.

## 571 **Surgical procedures**

572 Mice were implanted with cranial windows over auditory cortex. Briefly, mice were  
573 anaesthetized with 1.5 – 3% isoflurane and a 3-mm circular craniotomy was performed over the  
574 left auditory cortex (stereotaxic coordinates) using a 3-mm biopsy punch centered over the  
575 stereotaxic coordinates of A1 (70% of the distance between bregma and lambda, 4.3 mm lateral  
576 to the midline). An adeno-associated virus (AAV) vector encoding the calcium indicator  
577 GCaMP6s or GCaMP6m (AAV1.Syn.GCaMP6s.WPRE.SV40 or  
578 AAV1.Syn.GCaMP6m.WPRE.SV40, UPENN vector core) was injected (750 nl,  $\sim 1.89 \times 10^{-12}$   
579 genome copies·ml<sup>-1</sup>) at a 750µm depth from the surface of the brain at 60 nl min<sup>-1</sup> for expression  
580 in layer 2/3 neurons in A1. 3 injections were made at the same lateral distance but separated by  
581 0.5 mm in the anterior-posterior direction or 5 injections were made spread across the window  
582 (0.3 – 0.5 mm apart). The injection needle was left in place for 10 mins after the injection was  
583 complete before retraction. Injections were made using a pump (Pump 11 Elite, Harvard  
584 Apparatus, USA) and needles were pulled (P-97 Puller, Sutter Instruments, USA) glass pipettes  
585 (Harvard Apparatus, USA) with tip openings of 30 – 50 µm. After injection, a circular 3-mm  
586 diameter glass coverslip (size 0 or 1, Warner Instruments) was placed in the craniotomy and  
587 fixed in place using a mix of cyanoacrylate glue and dental cement. A custom-made stainless-  
588 steel head-plate (eMachine Shop) was fixed to the skull using C&B Metabond dental cement  
589 (Parkell). The implant was further secured using black dental cement. Mice were allowed to  
590 recover for 3 days post-surgery.

## 591 **Behavioral training and testing**

592 Mice underwent a minimum of 4 imaging sessions (range: 4 – 11) prior to differential auditory  
593 fear conditioning (DFC). DFC and subsequent fear retrieval testing took place in two different  
594 contexts (A and B, discussed below). Before and after each conditioning or retrieval, we cleaned  
595 the conditioning and testing chambers with either detergent (retrieval chamber) or 70% ethanol



596 (conditioning chamber). We recorded a video of the mouse in the testing chamber using  
597 FreezeFrame 3 software (Coulbourn) at 3.75 Hz; the subsequent movement index (mean  
598 grayscale values of frame ( $n+1$ ) minus the preceding frame ( $n$ )) was exported and analyzed  
599 offline using MATLAB. The threshold of movement was defined as the 12.5<sup>th</sup> percentile of the  
600 values from each session. The mouse was considered to be freezing if the movement index was  
601 below the threshold; the measure of freezing was expressed as a percentage of time spent  
602 freezing during stimulus presentation and for baseline during the 30s prior to stimulus onset.

603 Stimuli were generated using FreezeFrame 3 and presented at 70 dB SPL from an  
604 electrostatic speaker (ES-1, TDT) mounted above the animal. DFC took place in context A (Fig.  
605 1). Stimuli were 30 s in duration and were either a continuous pure tone (4 mice) or pulsed pure  
606 tones (500 ms duration at 1 Hz). The CS+ (15 kHz) was paired with a foot-shock (1 s, direct  
607 current, 0.7 mA, 10 pairings, inter-trial interval: 50 – 200 s) delivered through the floor of context  
608 A (by precision animal shocker, Coulbourn). The foot-shock either co-terminated with the  
609 continuous tone or the onset coincided with the final tone pulse of the CS+ stimuli. The CS- (11.4  
610 kHz) was presented after each CS+-foot-shock pairing but was not reinforced (10 presentations,  
611 inter-trial interval: 20 – 180 s). Fear memory retrieval sessions in context B followed each two-  
612 photon imaging session after conditioning. The CS+ and CS- were presented 4 times (30 s  
613 duration, interleaved, inter-trial interval: 30 – 180 s). For 4 mice, longer continuous presentations  
614 of the CS+ and CS- were presented (either 120 s, 1 mouse, or 60 s, 3 mice), for these mice,  
615 trials were divided into 4 equal durations and treated as above. In *pseudo*-conditioning, the foot-  
616 shocks were presented interleaved between the stimuli in periods of silence. Baseline freezing  
617 consisted of an equal time of silence prior to tone onset.

618 Conditioned mice that did not freeze either to CS+ or CS- were removed from subsequent  
619 analysis (two-way ANOVA for each mouse on freezing scores to CS+, CS- and baseline from all  
620 retrieval sessions (16 trials for each CS and 32 trials for baseline). Stimulus (CS+/CS-) and  
621 baseline (stimulus/no stimulus) were the independent variables. Learners were defined as those  
622 with significant effect of baseline or baseline\*stimulus,  $p < .05$ ). 6 mice (5 males, 1 female) were  
623 excluded from the study, leaving 15 conditioned mice (10 males, 5 females).

624 For each mouse the learning specificity ( $LS$ , Equation 1<sup>3</sup>) was calculated as:

625

$$LS = \sum_{i=1}^N fr_{CS^+}(i) / N - \sum_{i=1}^N fr_{CS^-}(i) / N$$

626 **Equation 1**

627 Where  $i$  is the trial index,  $fr_{CS+/-}(i)$  is the fraction of time spent freezing during trial  $i$  in the  
628 CS+/- condition, respectively, and  $N$  is the number of trials per condition.

629 **Calcium imaging procedure and acoustic stimuli**

630 All imaging sessions were carried out inside a single-walled acoustic isolation booth  
631 (Industrial Acoustics). Mice were placed in the imaging setup, and the head plate was secured  
632 to a custom base (eMachine Shop) serving to immobilize the head. Mice were gradually  
633 habituated to head-fixing over 3 – 5 days, 3 – 4 weeks after surgery and before imaging  
634 commenced. Imaging took place in mice aged 17.5 – 19.6 weeks (min: 12.9, max: 27.1 weeks).

635 We recorded changes in fluorescence of GCaMP6s/m caused by fluctuations in calcium  
636 concentration in transfected neurons of awake, head-fixed mice, using two-photon microscopy  
637 (Ultima *in vivo* multiphoton microscope, Bruker). We used a 16X Nikon objective with 0.8  
638 numerical aperture (Thorlabs, N16XLWD-PF). The laser (940 nm, Chameleon Ti-Sapphire)  
639 power at the brain surface was kept below 30 mW. Recordings were made at 512 x 512 pixels  
640 and 13-bit resolution at ~30 frames per second.

641 Stimuli were generated at a sampling rate of 400 kHz using MATLAB (MathWorks, USA)  
642 and consisted of 100-ms long tone pips in the 5–32-kHz frequency range presented at 60 – 80  
643 dB SPL. In a single recording session, each frequency was repeated 15 – 30 times in a *pseudo*-  
644 random order with a 4-s inter-stimulus interval.

645 **Cell tracking across imaging sessions.**

646 We imaged the activity from the same cells over 15 days in layers 2/3 of auditory cortex,  
647 using blood vessel architecture, depth from the surface, and the shape of cells to return to the  
648 same imaging site. To identify ROIs across imaging sessions that corresponded to the same  
649 cell, the maximum-projection fluorescence images from each day were registered by  
650 transforming the coordinates of landmarks present in both images in MATLAB (2017a) using the  
651 *fitgeotrans* function. The transformation was applied to ROIs from the second imaging session  
652 to match the first – all subsequent sessions were aligned to the first imaging session. We next  
653 calculated the distance between all the pairs of centroids (mean x-y position of each ROI) across  
654 the two sessions; ROIs from the two sessions were then automatically registered as the same  
655 cell based on the nearest centroid. We then manually checked the shape and position of the

656 ROIs for any pairs that had duplicate matches, <80% ROI overlap, or a larger than average  
657 distance between the centroid locations (>2 standard deviations). ROIs which were not matched  
658 to any earlier ROIs were counted as new cells. This process was repeated for subsequent  
659 sessions, registering the imaging field to the first session, and comparing the ROIs to the  
660 cumulative ROIs from previous sessions. A final manual inspection of all the unique ROIs was  
661 performed after all the imaging sessions were registered. ROIs that overlapped with each other  
662 extensively were excluded from the dataset since it was unclear whether they were the same or  
663 different cells. Examples of tracked cells and aligned ROIs are shown in Fig. S1.

## 664 **Data analysis and statistical procedures**

665 Publicly available toolboxes <sup>22</sup> running on MATLAB were used to register the two-photon  
666 images, select regions of interest (ROI), and estimate neuropil contamination, resulting in a  
667 neuropil-corrected fluorescence trace ( $F$ ) for each neuron. This trace was low pass filtered (filter  
668 cut off at 7.5 Hz) to remove high frequency noise. From this filtered trace, we calculated the  
669 mean baseline fluorescence ( $F_{baseline}$ ) and standard deviation of the baseline ( $F_{std}$ ) over the one  
670 second prior to tone onset, and then determined the change in fluorescence over time relative  
671 to the mean baseline fluorescence ( $\Delta F = F - F_{baseline}$ ) for each sound presentation. We then  
672 divided  $\Delta F$  by  $F_{std}$ , effectively calculating the z-score of the fluorescence response relative to the  
673 baseline ( $\Delta F/F_{std}$ ) for each sound presentation.

674 The response to each tone was defined as the mean  $\Delta F/F_{std}$  over 2 seconds following tone  
675 onset. Neurons were deemed sound responsive if at least one of the frequency responses was  
676 different from zero ( $t$ -test,  $p < 0.05$ , corrected for multiple comparisons using false discovery rate  
677 <sup>55,56</sup>). The frequency response function was defined as the mean response to each tone  
678 frequency across repeats. Best frequency was defined as the frequency with the highest mean  
679 response. Sparseness ( $S$ , Equation 2 <sup>29,30</sup>) was used to estimate the sharpness of response  
680 functions, with 1 being very sharply tuned and 0 being an equal response to each tone frequency:

$$681 \quad a = \frac{((\sum r_i)/N)^2}{\sum(r_i^2/N)} \quad S = \frac{1-a}{1-1/N}$$

### 682 **Equation 2**

683 where  $r_i$  is the mean response to the frequency  $i$  and  $N$  is the total number of frequencies  
684 tested.

685 The Z-scored difference between responses to CS+ and CS- ( $Z_{diff}$ , Equation 3) was  
686 calculated for each neuron using the following equation:

687 
$$Z_{diff} = \left| \frac{\sum r_{CS+}/N - \sum r_{CS-}/N}{\sqrt{(\sigma_{r_{CS+}} \cdot \sigma_{r_{CS-}})}} \right|$$

688 **Equation 3**

689 where  $r_{CS+/CS-}$  is the single trial mean responses (mean  $\Delta F/F_{std}$  over 2 s post-stimulus onset)  
690 to CS+ and CS- respectively,  $N$  is the number of repeats of each stimulus and  $\sigma$  is the standard  
691 deviation of mean responses. The  $Z_{diff}$  score was considered significant if the actual  $Z_{diff}$  was  
692 larger than the 95<sup>th</sup> percentile of the distribution of  $Z_{diff}$  scores calculated with shuffled the  
693 CS+/CS- response labels 250 times. For mice not tested under the two-photon directly with the  
694 CS+ or CS-, the data were linearly interpolated to estimate responses at CS- and CS+.

695 For fitting the Support Vector Machine, we used MATLAB's *fitcsvm* function with a Gaussian  
696 kernel and 10-fold cross-validation to predict the learning specificity based on the standardized  
697 single-trial population responses (mean  $\Delta F/F_{std}$  over 2 s post-stimulus onset for each neuron).  
698 We used a Gaussian kernel since it makes the least assumptions about the underlying  
699 distributions of population responses.

700 We calculated the confidence intervals of correlations using a bootstrap procedure,  
701 resampling, with replacement, the data 1000 times, and computing the Pearson's correlation  
702 between the resampled data. We defined the 95% confidence limits of the correlation coefficient  
703 ( $r$ ) as the 2.5<sup>th</sup> and 97.5<sup>th</sup> percentiles of the resulting distribution of correlation coefficients. In  
704 order to assess whether two correlations were significantly different from one another we  
705 subtracted the bootstrapped  $r$  distributions of each dataset from one another, the change in  $r$   
706 was considered significant if 95% CI of the difference-distribution did not overlap with zero.

707 To compare results between testing groups (conditioned/*pseudo*-conditioned) we used two-  
708 way repeated measures ANOVAs with the relevant variables (see Tables S1, S3-13, S16, S19-  
709 22,).

710 For mice that were not tested at 11.4 and 15 kHz under the two-photon microscope (4  
711 conditioned mice) responses were interpolated from the frequency response functions pre- and  
712 post-DFC. For cells present in more than one session either pre- or post-DFC, the frequency

713 response curves from each session were averaged and the changes in response were assessed  
714 from the mean across pre- and post-DFC sessions. For comparing the fluorescence traces of  
715 responses (Fig. S6D-G), for the 4 mice not tested directly at CS+ and CS-, the nearest  
716 frequencies were used.

## 717 **Confirming anatomical location of recording**

718 Upon conclusion of the imaging sessions, we removed the windows of the mice and injected  
719 a red fluorescent marker (Red Retrobeads, CTB or AAV5.CAG.hChR2(H134R)-  
720 mCherry.WPRE.SV40 (mCherry)) into the site of imaging as identified by blood vessel patterns.  
721 Briefly, we anaesthetized mice with 1.5 – 3% isoflurane and used a drill (Dremel) to remove the  
722 dental cement holding the window in place. We removed the glass window and injected the red  
723 marker into the imaging site (Red Retrobeads: 250 nl, CTB: 500 nl (0.5%), mCherry: 500 nl)  
724 using a glass pipette (tip diameter: 40 – 50  $\mu\text{m}$ ) at 60 nl min<sup>-1</sup>. Following the injection, we covered  
725 the exposed brain with silicon (Kwik-Sil, World Precision Instruments) and then coated it with  
726 dental cement. After allowing time for retrograde transport (retrobeads and CTB: 1 week) or viral  
727 transfection and expression (mCherry: 3 weeks) mice were deeply anesthetized with a mixture  
728 of Dexmedetomidine (3 mg/kg) and Ketamine (300 mg/kg) and brains were extracted following  
729 perfusion in 0.01 M phosphate buffer pH 7.4 (PBS) and 4% paraformaldehyde (PFA). They were  
730 further fixed in PFA overnight and cryopreserved in 30% sucrose solution for 2 days before  
731 slicing. The location of imaging was confirmed through fluorescent imaging (Fig. S2). For  
732 Retrobeads and CTB, the injection site was clear as a very bright injection site, for mCherry,  
733 expression levels were measured across the AC and the site of imaging was assumed to be the  
734 section with the strongest expression/brightest red. The identified sections were cross-  
735 referenced with the Allen Institute Mouse Brain Atlas using freely available software <sup>57</sup>.

## 736 **Model**

### 737 ***Neuron model and network***

738 We simulated cortical neuronal populations, MGB populations and a BLA neuronal  
739 population in a rate-based description of neuronal activity. We simulated  $N = 10$  MGB  
740 populations. Each MGB population receives  $N = 10$  inputs  $x_i^{MGB}$ ,  $i = 1..N$ . To model the fact that  
741 neighboring inputs are correlated, we generated the inputs  $x_i$  assuming that they each have a  
742 similar tuning to stimuli. These stimuli were modeled as 10 time-dependent activities  $s_j(t)$  (which

743 corresponded to a sound amplitude at a given frequency,  $j$ ). The activity of input  $i$  was calculated  
744 by a sum of the stimulus channels, weighted with tuning strengths  $x^{MGB}_i(t) = \sum_j T^{MGB}_{ij} s_j(t) +$   
745  $x^{ctx}_j(t)$ . The input tuning was Gaussian:  $T^{MGB}_{ij} = \left[ e^{-\frac{(i-j)^2}{2\sigma^{MGB}}} \right]_+$  for  $i$  and  $j$  going from 1 to 10.  
746  $[\cdot]_+$  means that negative values are set to zeros. The term  $x^{ctx}$  corresponds to the direct cortical  
747 feedback. The parameter  $\sigma^{MGB}$  regulated how broad the population response is to the sound. In  
748 the model, we assumed that MGB neuronal populations always have a small overlap in neuronal  
749 responses ( $\sigma^{MGB} = 0.8$ ).

750 Similarly, we simulated  $N = 10$  cortical populations as  $x^{ctx}_i(t) = \sum_j T^{ctx}_{ij} x^{MGB}_j(t)$ . The  
751 input tuning was also Gaussian:  $T^{ctx}_{ij} = \frac{1}{1.8} \left[ e^{-\frac{(i-j)^2}{2\sigma^{ctx}}} - I^{ctx} \right]_+$  for  $i$  and  $j$  from 1 to 10.  $I^{ctx} = 0.9$   
752 was a broad inhibitory term.

753 In the simulations, we tested for two different values of  $\sigma^{ctx}$ ; one corresponding to narrow  
754 tuning with a small overlap ( $\sigma^{ctx} = 3$ ), and one corresponding to broad tuning with a large overlap  
755 ( $\sigma^{ctx} = 10$ ). (Note that  $\sigma^{MGB} = 0.8$  was equivalent to  $\sigma^{ctx} = 3$  since we did not model MGB  
756 inhibition here,  $I^{MGB} = 0$ ). To avoid boundary effects, we had a circular boundary condition of the  
757 10 inputs, meaning that input 1 and input 10 are neighbors.

758 Finally, we simulated one population in the BLA. It received inputs from both cortical and  
759 MGB populations, i.e.,  $y = w^{MGB} x^{MGB} + w^{ctx} x^{ctx}$ , where  $w^{MGB}$  are the weights from MGB  
760 neurons to the BLA neurons, and  $w^{ctx}$  are the weights from cortical neurons to the BLA.  
761 Normalized freezing response was computed as the activity after the fear conditioning paradigm  
762 (see below) normalized by the maximal activity (i.e., when the weights are all 1).

### 763 **Modelling fear conditioning paradigm and interventions**

764 During the fear conditioning training to simulate a CS- tone, we set (channel number 6)  $s_6 =$   
765 1, all the other inputs to zero, and a CS+ we set (channel number 3)  $s_3 = 1$ , all the other inputs  
766 to zero. In addition, we paired it with a shock ( $e = 1$  if there is a shock,  $e = 0$  otherwise). The  
767 synaptic weights were plastic under the following rules:  $\Delta w^{ctx/MGB}_i = \alpha x^{ctx/MGB}_i e$ , where  $\alpha =$   
768 0.1 is the learning rate. This is analogous to the standard Delta rule. The weights were bound  
769 between 0 and 1 and are initialized at 0.1. We simulated the fear conditioning for 10 time-steps  
770 [arbitrary time]. To simulate optogenetic inactivation of PV neurons in AC<sup>12</sup>, which decreases

771 inhibition in AC, we lowered inhibition in AC by setting  $I^{ctx} = 0.45$  (half the ‘normal’ level), the  
772 maximum freezing was computed with the original inhibitory term intact ( $I^{ctx} = 0.9$ ). To simulate  
773 pharmacological inactivation of AC during memory recall (after learning), we tested the behavior  
774 of the model with AC inactivation by setting  $x_i^{ctx} = 0$  during the BLA simulation protocol.

## 775 **Data availability**

776 All data and the code to generate the figures as well as the model are available in free  
777 access here: <https://doi.org/10.5061/dryad.wpzqmsbhw> .

778 REVIEWER LINK:

779 <https://datadryad.org/stash/share/Cjd1A7BkhvPg2aNETgh3PAoAayMgRT0vIACCtSpBcTA>

780

## 781 **Supplemental Information (12 figures and 22 tables)**

782 Figure S1: Longitudinal two-photon imaging tracks activity of neurons over weeks.

783 Figure S2: Location of imaging site example.

784 Figure S3: Mean freezing to CS+ and CS- and learning specificity across sessions.

785 Figure S3: Change in  $Z_{diff}$  in tracked cells between consecutive sessions.

786 Figure S4: Mean response to CS+ or CS- does not predict learning specificity.

787 Figure S5: Changes in neuronal discrimination over consecutive imaging sessions.

788 Figure S6: Changes in frequency response after conditioning.

789 Figure S7: Changes in normalized responses do not correlate with learning specificity.

790 Figure S8: Changes in neuronal discriminability negatively correlate with learning specificity.

791 Figure S9: Model schematic.

792 Figure S10: Model schematic with PV inactivation of AC during DFC Figure S11: Model  
793 schematic with AC inactivation during memory recall.

794 Figure S12: Auditory Brainstem Responses.

795 Table S1: Statistics for Fig. S3B-C.

796 Table S2: Statistics for Fig. 1C.

- 797 Table S3: Statistics for Fig. 4A
- 798 Table S4: Statistics for Fig. 4B
- 799 Table S5: Statistics comparing change in SVM performance over consecutive sessions.
- 800 Table S6: Statistics comparing change in Zdiff over consecutive sessions.
- 801 Table S7: Statistics for Fig. 5A (left panel).
- 802 Table S8: Statistics for Fig. 5A (middle panel).
- 803 Table S9: Statistics for Fig. 5A (right panel).
- 804 Table S10: Statistics for Fig. 5B Table
- 805 S11: Statistics for Fig. 5C
- 806 Table S12: Statistics comparing normalized responses to conditioned stimuli in conditioned  
807 and pseudo-conditioned mice from pre- to post-DFC.
- 808 Table S13: Statistics for Fig. S6B:
- 809 Table S14: Change in negative responses of the lower quartile of responding neurons from  
810 pre- to post-DFC in conditioned mice (Fig. S6E).
- 811 Table S15: Change in negative responses of the upper quartile of responding neurons from  
812 pre- to post-DFC in conditioned mice (Fig. S6E).
- 813 Table S16: Statistics for Fig. S6C.
- 814 Table S17: Change in negative responses of the lower quartile of responding neurons from  
815 pre- to post-DFC in pseudo-conditioned mice (Fig. S6G).
- 816 Table S18: Change in negative responses of the upper quartile of responding neurons from  
817 pre- to post-DFC in pseudo-conditioned mice (Fig. S6G).
- 818 Table S19: Statistics comparing non-normalized responses to conditioned stimuli in  
819 conditioned and pseudo-conditioned mice from pre- to post-DFC.
- 820 Table S20: Statistics for Fig. 6A & B.
- 821 Table S21: Statistics for Fig. 6C.
- 822 Table S22: Statistics for Fig. 6D.



## 823 **References**

- 824 1. Quirk, G. J., Armony, J. L. & LeDoux, J. E. Fear conditioning enhances different temporal  
825 components of tone-evoked spike trains in auditory cortex and lateral amygdala. *Neuron*  
826 **19**, 613–624 (1997).
- 827 2. Johansen, J. P., Cain, C. K., Ostroff, L. E. & LeDoux, J. E. Molecular Mechanisms of Fear  
828 Learning and Memory. *Cell* **147**, 509–524 (2011).
- 829 3. Aizenberg, M. & Geffen, M. N. Bidirectional effects of aversive learning on perceptual  
830 acuity are mediated by the sensory cortex. *Nat. Neurosci.* **16**, 994–6 (2013).
- 831 4. Resnik, J., Sobel, N. & Paz, R. Auditory aversive learning increases discrimination  
832 thresholds. *Nat. Neurosci.* **14**, 791–796 (2011).
- 833 5. Li, W., Howard, J. D., Parrish, T. B. & Gottfried, J. A. Aversive learning enhances  
834 perceptual and cortical discrimination of indiscriminable odor cues. *Science (80-. ).* **319**,  
835 1842–1845 (2008).
- 836 6. Chapuis, J. & Wilson, D. a. Bidirectional plasticity of cortical pattern recognition and  
837 behavioral sensory acuity. *Nature Neuroscience* **15**, 155–161 (2011).
- 838 7. Mahan, A. L. & Ressler, K. J. Fear conditioning, synaptic plasticity and the amygdala:  
839 Implications for posttraumatic stress disorder. *Trends in Neurosciences* **35**, 24–35 (2012).
- 840 8. Jovanovic, T. & Ressler, K. J. How the neurocircuitry and genetics of fear inhibition may  
841 inform our understanding of PTSD. *American Journal of Psychiatry* **167**, 648–662 (2010).
- 842 9. Krusemark, E. A. & Li, W. Enhanced olfactory sensory perception of threat in anxiety: An  
843 event-related fMRI study. *Chemosens. Percept.* **5**, 37–45 (2012).
- 844 10. Letzkus, J. *et al.* A disinhibitory microcircuit for associative fear learning in the auditory

- 845 cortex. *Nature* **480**, 331–336 (2011).
- 846 11. Dalmy, T. *et al.* A Critical Role for Neocortical Processing of Threat Memory. *Neuron* 1–  
847 15 (2019). doi:10.1016/J.NEURON.2019.09.025
- 848 12. Aizenberg, M., Mwilambwe-Tshilobo, L., Briguglio, J. J., Natan, R. G. & Geffen, M. N.  
849 Bidirectional Regulation of Innate and Learned Behaviors That Rely on Frequency  
850 Discrimination by Cortical Inhibitory Neurons. *PLOS Biol.* **13**, e1002308 (2015).
- 851 13. Ceballo, S., Piwkowska, Z., Bourg, J., Daret, A. & Bathellier, B. Targeted Cortical  
852 Manipulation of Auditory Perception. *SSRN Electron. J.* **104**, 1168-1179.e5 (2019).
- 853 14. Wigstrand, M. B., Schiff, H. C., Fyhn, M., LeDoux, J. E. & Sears, R. M. Primary auditory  
854 cortex regulates threat memory specificity. *Learn. Mem.* **24**, 55–58 (2017).
- 855 15. Weinberger, N. M. Specific long-term memory traces in primary auditory cortex. *Nat. Rev.*  
856 *Neurosci.* **5**, 279–290 (2004).
- 857 16. Weinberger, N. M. & Diamond, D. M. Physiological plasticity in auditory cortex: Rapid  
858 induction by learning. *Prog. Neurobiol.* **29**, 1–55 (1987).
- 859 17. Edeline, J.-M. & Weinberger, N. M. Receptive field plasticity in the auditory cortex during  
860 frequency discrimination training: Selective retuning independent of task difficulty. *Behav.*  
861 *Neurosci.* **107**, 82–103 (1993).
- 862 18. Gillet, S. N., Kato, H. K., Justen, M. A., Lai, M. & Isaacson, J. S. Fear learning regulates  
863 cortical sensory representations by suppressing habituation. *Front. Neural Circuits* **11**, 112  
864 (2018).
- 865 19. Ohl, F. W. & Scheich, H. Differential frequency conditioning enhances spectral contrast  
866 sensitivity of units in auditory cortex (field AI) of the alert Mongolian gerbil. *Eur. J. Neurosci.*

- 867           **8**, 1001–17 (1996).
- 868   20.   Chen, T.-W. *et al.* Ultrasensitive fluorescent proteins for imaging neuronal activity. *Nature*  
869           **499**, 295–300 (2013).
- 870   21.   Staib, M. & Bach, D. R. Stimulus-invariant auditory cortex threat encoding during fear  
871           conditioning with simple and complex sounds. *Neuroimage* **166**, 276–284 (2018).
- 872   22.   Pachitariu, M. *et al.* *Suite2p: beyond 10,000 neurons with standard two-photon*  
873           *microscopy. bioRxiv* **53**, (Cold Spring Harbor Labs Journals, 2017).
- 874   23.   Georgopoulos, A. P., Schwartz, A. B. & Kettner, R. E. Neuronal Population Coding of  
875           Movement Direction. *Science* **233**, 1416–1419 (1986).
- 876   24.   Stringer, C. *et al.* Spontaneous behaviors drive multidimensional, brainwide activity.  
877           *Science (80-. )*. **364**, (2019).
- 878   25.   Runyan, C. A., Piasini, E., Panzeri, S. & Harvey, C. D. Distinct timescales of population  
879           coding across cortex. *Nature* **548**, 92–96 (2017).
- 880   26.   Kato, H. K., Gillet, S. N. & Isaacson, J. S. Flexible Sensory Representations in Auditory  
881           Cortex Driven by Behavioral Relevance. *Neuron* **88**, 1027–1039 (2015).
- 882   27.   Ohl, F. W. & Scheich, H. Learning-induced dynamic receptive field changes in primary  
883           auditory cortex of the unanaesthetized Mongolian gerbil. *J. Comp. Physiol. A Sensory,*  
884           *Neural, Behav. Physiol.* **181**, 685–696 (1997).
- 885   28.   Ohl, F. W. & Scheich, H. Fallacies in behavioural interpretation of auditory cortex plasticity.  
886           *Nat. Rev. Neurosci.* **5**, 1–1 (2004).
- 887   29.   Rust, N. C. & DiCarlo, J. J. Balanced Increases in Selectivity and Tolerance Produce  
888           Constant Sparseness along the Ventral Visual Stream. *J. Neurosci.* **32**, 10170–10182

- 889 (2012).
- 890 30. Blackwell, J. M., Lesicko, A. M., Rao, W., De Biasi, M. & Geffen, M. N. Auditory cortex  
891 shapes sound responses in the inferior colliculus. *Elife* **9**, (2020).
- 892 31. Briguglio, J. J., Aizenberg, M., Balasubramanian, V. & Geffen, M. N. Cortical Neural Activity  
893 Predicts Sensory Acuity Under Optogenetic Manipulation. *J. Neurosci.* **38**, 2094–2105  
894 (2018).
- 895 32. Pooresmaeili, A., Poort, J., Thiele, A. & Roelfsema, P. R. Separable Codes for Attention  
896 and Luminance Contrast in the Primary Visual Cortex. *J. Neurosci.* **30**, 12701–12711  
897 (2010).
- 898 33. Talwar, S. K. & Gerstein, G. L. Reorganization in awake rat auditory cortex by local  
899 microstimulation and its effect on frequency-discrimination behavior. *J. Neurophysiol.* **86**,  
900 1555–1572 (2001).
- 901 34. Maor, I. *et al.* Neural Correlates of Learning Pure Tones or Natural Sounds in the Auditory  
902 Cortex. *Front. Neural Circuits* **13**, 82 (2020).
- 903 35. He, J. Corticofugal modulation of the auditory thalamus. *Exp. Brain Res.* **153**, 579–590  
904 (2003).
- 905 36. Williamson, R. S. & Polley, D. B. Parallel pathways for sound processing and functional  
906 connectivity among layer 5 and 6 auditory corticofugal neurons. *Elife* **8**, (2019).
- 907 37. Suga, N. Role of corticofugal feedback in hearing. *J. Comp. Physiol. A* **194**, 169–183  
908 (2008).
- 909 38. Aizenberg, M. *et al.* Projection from the Amygdala to the Thalamic Reticular Nucleus  
910 Amplifies Cortical Sound Responses. *Cell Rep.* **28**, 605-615.e4 (2019).

- 911 39. Betley, J. N., Cao, Z. F. H., Ritola, K. D. & Sternson, S. M. Parallel, Redundant Circuit  
912 Organization for Homeostatic Control of Feeding Behavior. *Cell* **155**, 1337–1350 (2013).
- 913 40. Zhang, G.-W. *et al.* A Non-canonical Reticular-Limbic Central Auditory Pathway via Medial  
914 Septum Contributes to Fear Conditioning. *Neuron* **97**, 406-417.e4 (2018).
- 915 41. Boatman, J. A. & Kim, J. J. A thalamo-cortico-amygdala pathway mediates auditory fear  
916 conditioning in the intact brain. *Eur. J. Neurosci.* **24**, 894–900 (2006).
- 917 42. Atencio, C., Sharpee, T. & Schreiner, C. Receptive field dimensionality increases from the  
918 auditory midbrain to cortex. *J. Neurophysiol.* (2012). doi:10.1152/jn.01025.2011
- 919 43. Linden, J. F. & Schreiner, C. E. Columnar Transformations in Auditory Cortex? A  
920 Comparison to Visual and Somatosensory Cortices. *Cereb. Cortex* **13**, 83–89 (2003).
- 921 44. Blackwell, J. M. & Geffen, M. N. Progress and challenges for understanding the function  
922 of cortical microcircuits in auditory processing. *Nat. Commun.* **8**, 1–9 (2017).
- 923 45. Wood, K. C., Blackwell, J. M. & Geffen, M. N. Cortical inhibitory interneurons control  
924 sensory processing. *Current Opinion in Neurobiology* **46**, 200–207 (2017).
- 925 46. Harris, K. D. & Shepherd, G. M. G. The neocortical circuit: themes and variations. *Nat.*  
926 *Neurosci.* **18**, 170–181 (2015).
- 927 47. Kuo, R. I. & Wu, G. K. The Generation of Direction Selectivity in the Auditory System.  
928 *Neuron* **73**, 1016–1027 (2012).
- 929 48. O'Sullivan, C., Weible, A. P. & Wehr, M. Auditory Cortex Contributes to Discrimination of  
930 Pure Tones. *eneuro* **6**, ENEURO.0340-19.2019 (2019).
- 931 49. Betzel, R. F., Wood, K. C., Angeloni, C., Neimark Geffen, M. & Bassett, D. S. Stability of  
932 spontaneous, correlated activity in mouse auditory cortex. *PLOS Comput. Biol.* **15**,

- 933 e1007360 (2019).
- 934 50. Dunsmoor, J. E. & Paz, R. Fear Generalization and Anxiety: Behavioral and Neural  
935 Mechanisms. *Biological Psychiatry* **78**, 336–343 (2015).
- 936 51. Ginat-Frolich, R., Klein, Z., Katz, O. & Shechner, T. A novel perceptual discrimination  
937 training task: Reducing fear overgeneralization in the context of fear learning. *Behav. Res.*  
938 *Ther.* **93**, 29–37 (2017).
- 939 52. Lange, I. *et al.* Behavioral pattern separation and its link to the neural mechanisms of fear  
940 generalization. *Soc. Cogn. Affect. Neurosci.* **12**, 1720–1729 (2017).
- 941 53. Roesmann, K. *et al.* Fear generalization of implicit conditioned facial features – Behavioral  
942 and magnetoencephalographic correlates. *Neuroimage* **205**, 116302 (2020).
- 943 54. Tuominen, L. *et al.* The relationship of perceptual discrimination to neural mechanisms of  
944 fear generalization. *Neuroimage* **188**, 445–455 (2019).
- 945 55. Groppe, D. fdr\_bh ([https://www.mathworks.com/matlabcentral/fileexchange/27418-](https://www.mathworks.com/matlabcentral/fileexchange/27418-fdr_bh)  
946 [fdr\\_bh](https://www.mathworks.com/matlabcentral/fileexchange/27418-fdr_bh)). *MATLAB Cent. File Exch.* (2020).
- 947 56. Benjamini, Y. & Hochberg, Y. Controlling the False Discovery Rate: A Practical and  
948 Powerful Approach to Multiple Testing. *J. R. Stat. Soc. Ser. B* **57**, 289–300 (1995).
- 949 57. Shamash, P., Carandini, M., Harris, K. & Steinmetz, N. A tool for analyzing electrode tracks  
950 from slice histology. *bioRxiv* 447995 (2018). doi:10.1101/447995

951